UNCLASSIFIED

AD NUMBER

ADB205827

NEW LIMITATION CHANGE

TO

Approved for public release, distribution unlimited

FROM

Distribution authorized to DoD only. Other requests shall be referred to Embassy of Australia, Head Pub. Sec. Def/Sci., 1601 Massachusetts Ave., NW, Washington, DC 20036.

AUTHORITY

DSTO ltr, 26 Mar 2002

THIS PAGE IS UNCLASSIFIED

LIMITED RELEASE

AR-008-994

DSTO-RR-0019

A Finite Difference Time Domain Calculation for Rotationally Symmetric Ultrawideband Antennas

Geoff Staines and Sean Braidwood

DTIC
ELECTE
DEC 27 1995
S D
F

Distribution is limited to officers of the Defence Departments of Australia, UK, USA, Others should refer to Document Exchange Centre, DIS Network Office, CP2-5-08, CANBERRA ACT 2600 AUSTRALIA

19951219 044

DTIC QUALITY INSPECTED 1

DEPARTMENT OF DEFENCE
DEFENCE SCIENCE AND TECHNOLOGY ORGANISATION

LIMITED RELEASE

~~DISTRIBUTION STATEMENT B:~~ Distribution authorized to DoD Components only
. Other requests shall be referred to

Embassy of Australia
Attn: Joan Bliss
Head. Pub. Sec.-Def/Sci.
1601 Massachusetts Ave., NW
Washington, DC 20036

A Finite Difference Time Domain Calculation for Rotationally Symmetric Ultrawideband Antennas

Geoff Staines and Sean Braidwood

Electronic Warfare Division
Electronics and Surveillance Research Laboratory

DSTO-RR-0019

ABSTRACT

A finite difference time domain (FDTD) technique for the analysis of ultrawideband (UWB) antennas with rotational symmetry has been developed. The theory is intended to treat various types of biconical antennas, and a mode matching analysis of spherically-capped bicones has been performed to verify the correct implementation of the FDTD calculation. In addition, experimental results have been obtained which are compared to the theoretical results. The FDTD software can be used for the design of high-power, directive UWB antennas with low sidelobe leakage for high-power UWB radar and electronic countermeasures applications.

RELEASE LIMITATION

~~*Access additional to the initial distribution is limited to the Defence Community of Australia, US and UK. Others MUST be referred to Chief, Electronic Warfare Division, ESRL.*~~

DEPARTMENT OF DEFENCE

DEFENCE SCIENCE AND TECHNOLOGY ORGANISATION

Published by

DSTO Electronics and Surveillance Research Laboratory
PO Box 1500
Salisbury South Australia 5108

Telephone: (08) 259 5181
Fax: (08) 259 5938

© Commonwealth of Australia 1994
AR-008-994
February 1995

Conditions of Release and Disposal

1. *This document is the property of the Australian Government; the information it contains is released for defence purposes only and must not be disseminated beyond the stated distribution without prior approval.*

2. *The document and information it contains must be handled in accordance with security regulations applying in the country of lodgement, downgrading instructions must be observed and delimitation is only with specific approval of the Releasing Authority as given in the Secondary Distribution statement.*

3. *This information may be subject to privately owned rights.*

4. *The officer in possession of this document is responsible for its safe custody. When no longer required this document should be destroyed and notification sent to: Senior Librarian, Defence Science and Technology Organisation Salisbury Research Library.*

A Finite Difference Time Domain Calculation for Rotationally Symmetric Ultrawideband Antennas

EXECUTIVE SUMMARY

A finite difference time domain (FDTD) technique has been developed for analysing rotationally symmetric ultrawideband (UWB) antennas of arbitrary cross section. This includes conventional biconical antennas. The restriction to rotationally symmetric antennas means that a 2 dimensional calculation is possible, reducing the required computational effort for realistic antennas to within practical limits.

For high power UWB applications such as impulse radar and disruption of electronic systems, compact, directive antennas with high breakdown voltages are required. The FDTD approach allows both the antenna and its feed to be accurately modelled. The technique can also be used to predict the characteristics of narrowband antennas for more conventional applications.

The correct implementation of the theory is verified by the analysis of a 9 mm conical D-dot sensor used for transient electromagnetics research at DSTO. Measured results are presented which agree well with the predictions of the FDTD analysis. In addition, a mode matching technique capable of analysing conventional biconical antennas is used to check the FDTD calculation. For the conical D-dot sensor, the agreement between the FDTD and mode matching techniques is excellent.

Accesion For
NTIS CRA&I ☐
DTIC TAB ☑
Unannounced ☐
Justification
By
Distribution /
Availability Codes
Dist | Avail and / or Special
14

THIS PAGE INTENTIONALLY BLANK

Authors

Geoff Staines
Electronic Warfare Division

Geoff Staines received the BSc (Physics) degree from the University of Queensland in 1987, the BSc(Hons) from Flinders University in 1988, and a PhD in plasma physics from Flinders University in 1991. Since 1992, he has been a research scientist in Advanced Concepts Group, Electronic Warfare Division, DSTO Salisbury.

Sean Braidwood
Electronic Warfare Division

Sean Braidwood received the BSc.(Hons) from Adelaide University in 1989 and a MSc. in atomic physics from Flinders University in 1993. He is currently working for Advanced Concepts Group in Electronic Warfare Division, DSTO Salisbury.

THIS PAGE INTENTIONALLY BLANK

Contents

1.	INTRODUCTION	1
2.	THE FINITE DIFFERENCE TIME DOMAIN (FDTD) METHOD	2
2.1	Introduction	2
2.2	The Yee Algorithm	2
	2.2.1 Mesh Equations	2
	2.2.2 Boundary Conditions	4
	2.2.2.1 Edge Boundary Conditions	4
	2.2.2.2 Antenna Feed	7
	2.2.2.3 Conducting Surface Boundary Conditions	9
2.3	The Contour Path (CP) Approach	10
	2.3.1 Mesh Equations	10
	2.3.2 Boundary Conditions	13
	2.3.2.1 Horizontal Cell Deformation	14
	2.3.2.1 Vertical Cell Deformation	15
2.5	Far Field Calculation	17
2.6	Energy Calculation	24
2.7	Coarse Outer Mesh	25
2.8	Summary	27
3.	CONICAL MONOPOLE D-DOT SENSOR ANALYSIS	27
3.1	Introduction	27
3.2	Reflected Voltage	28
3.3	Transmit Response	31
3.4	Receive Response	34
3.5	Comparison of FDTD D-dot Response with Experiment	37
4.	CONCLUSIONS	39
APPENDIX A		
	SPHERICALLY CAPPED CONICAL MONOPOLE ANALYSIS	41
A.1	Spherical Eigenmodes	42
A.2	Aperture Field Matching	48
A.3	Power Conservation	53
A.4	Small Conical Monopole Approximation	55
A.5	Transfer Functions	57
A.6	Time Domain Response	60
A.7	Summary	62
A.8	References	63

Figure 2.1:	Interleaved electric and magnetic fields for FDTD grid cell.	3
Figure 2.2:	Truncated mesh in cylindrical geometry	5
Figure 2.3:	Staircased conducting boundaries	9
Figure 2.4:	Ampere and Faraday contour geometry for Contour Path technique	11
Figure 2.5	Horizontal cell deformation near conducting surface	15
Figure 2.6:	Vertical cell deformation near conducting surface	16
Figure 2.7:	Fine/coarse mesh interface detail	26
Figure 3.1:	Conical monopole geometry	28
Figure 3.2:	Reflected voltage from ideal, full analytic, and FDTD calculations for tp = 50 ps	30
Figure 3.3:	Reflected voltage from ideal, full analytic, and FDTD calculations for tp = 100 ps	30
Figure 3.4:	Reflected voltage from ideal, full analytic, and FDTD calculations for tp = 250 ps	31
Figure 3.5:	FDTD, full and ideal analytic, and first order far field comparison for tp = 50 ps	32
Figure 3.6:	FDTD, full and ideal analytic, and first order far field comparison for tp = 100 ps	33
Figure 3.7:	FDTD, full and ideal analytic, and first order far field comparison for tp = 250 ps	33
Figure 3.8:	FDTD, full and ideal analytic, and first order receive voltage for tp = 50 ps	35
Figure 3.9:	FDTD, full and ideal analytic, and first order receive voltage for tp = 100 ps	36
Figure 3.10:	FDTD, full and ideal analytic, and first order receive voltage for tp = 250 ps	36
Figure 3.11:	Measured and predicted conical D-dot sensor output voltage	37
Figure 3.12:	Reconstructed and predicted incident field	38
Figure A.1:	Conical monopole geometry	41
Figure A.2:	Transmission transfer function of matched conical monopole	59
Figure A.3:	Reception transfer function per unit antenna length for matched conical monopole	59
Figure A.4:	Radiated field from 50 W conical monopole for various a/tw.	61
Figure A.5:	Voltage across 50 W conical monopole receive antenna for various a/tw.	62

1. Introduction

High-power ultrawideband (UWB) systems are under consideration for applications in radar and electronic countermeasures [1-4]. Modern electronic systems commonly used for military purposes are increasingly vulnerable to high-power emissions such as UWB radiation due to the increasing use of large scale integrated circuits and other solid state components.

High-power UWB radiation is generated using a suitable broadband antenna excited by a voltage transient. The essential component of the generator used to provide the electrical transient is a high-power switch capable of producing subnanosecond output pulse risetimes. Photoconductive solid state switches [1, 3, 5, 6] or spark gap devices [1, 7, 8] are suitable for this purpose. While high-power UWB generators are both available and affordable, one of the most critical hardware items for a practical UWB system is the antenna. There are several important requirements for a useable antenna:

(i) High breakdown voltage (> 100 kV) in order to radiate sufficiently large voltage transients to detect (for radar) or disrupt (for countermeasures) targets at useful ranges. This apparently ambitious requirement is mitigated somewhat since the voltage peaks across the antenna for approximately a nanosecond or less, and so the pulse breakdown voltage is up to an order of magnitude higher than the DC breakdown voltage.

(ii) High directivity in order to maximise the power incident on the target, while avoiding irradiation of nearby friendly or neutral targets. The directivity is ultimately limited by the maximum permissible size of the antenna aperture as dictated by host platform constraints.

(iii) Low sidelobes in order to minimise the possibility of damage to or disruption of the host platform. While hardening of the host platform is possible, the cost and effort required is minimised by the use of a low-sidelobe antenna. This goal is the most difficult to achieve since the antenna must cover a very large bandwidth (typically greater than 25% of the centre frequency), while being non-dispersive (no distortion of pulse shape).

Since fully three-dimensional electromagnetic field calculations require a substantial computational effort, effectively two-dimensional rotationally symmetric antennas such as the bicone were chosen for detailed study. All of the previously mentioned aspects of high power UWB antenna design can be investigated using a straightforward finite difference time domain (FDTD) algorithm requiring a modest computational effort. This report describes the development of this FDTD technique, together with initial results relating to the analysis of small spherically-capped conical monopole D-dot sensors. These results include a comparison of results obtained

from the FDTD analysis and an analytic mode matching technique for these sensors. Experimental results are included to show that the FDTD technique successfully predicts the correct dependence of the sensor output voltage on the angle of incidence of the applied field. A detailed derivation of the analytic technique is presented in Appendix A.1.

2. The Finite Difference Time Domain (FDTD) Method

2.1 Introduction

There are currently two categories of time domain numerical techniques commonly used for analysing UWB antennas. The first type are the integral equation methods such as the electric field integral equation (EFIE) method developed by Rao [9, 10]. Conducting surfaces are modelled by planar triangular or rectangular patches, and the method of moments is applied in the time domain to calculate the current densities over these surfaces. The second type consists of the finite difference time domain (FDTD) method first proposed by Yee [11]. This technique is used to determine the fields in a volume surrounded by a surface on which a boundary condition is imposed. Maxwell's equations are discretised spatially and temporally, and the fields in the volume are solved on a time-marching finite difference mesh. The FDTD method has the advantages of simplicity and generality over integral equation methods, although at the expense of a larger computational effort, since the electromagnetic field in a three-dimensional volume is being calculated as opposed to the current density over two-dimensional surfaces. The memory requirement is alleviated by considering only two dimensional azimuthally symmetric antenna structures.

2.2 The Yee Algorithm

2.2.1 Mesh Equations

Since the antennas are rotationally symmetric, the analysis can be reduced to a two-dimensional problem by adopting cylindrical coordinates [12-14]. Since the excitation for the rotationally-symmetric antenna is a TEM mode, only TM modes will be excited. In cylindrical geometry, these modes have field components E_r, E_z, and H_ϕ only. Maxwell's time dependent curl equations relating these quantities are

$$\frac{\partial E_r}{\partial z} - \frac{\partial E_z}{\partial r} = -\mu_0 \frac{\partial H_\phi}{\partial t} \tag{1}$$

$$-\frac{\partial H_\phi}{\partial z} = \varepsilon \frac{\partial E_r}{\partial t} \tag{2}$$

$$\frac{1}{r}\frac{\partial(rH_\phi)}{\partial r} = \varepsilon\frac{\partial E_z}{\partial t} \tag{3}$$

where ε is the permittivity at the field point, and μ_0 is the permeability.

The field quantities are discretised in the spatial and time coordinates for representation on a finite difference mesh. For spatial increments Δ_r, and Δ_z, and time increment Δ_t, the notation for field quantity Q at the point (r_i, z_j) at time t_n is

$$\begin{aligned} Q^n(i,j) &= Q(r_i, z_j, t_n) \\ &= Q(i\Delta_r, j\Delta_z, n\Delta_t) \end{aligned}$$

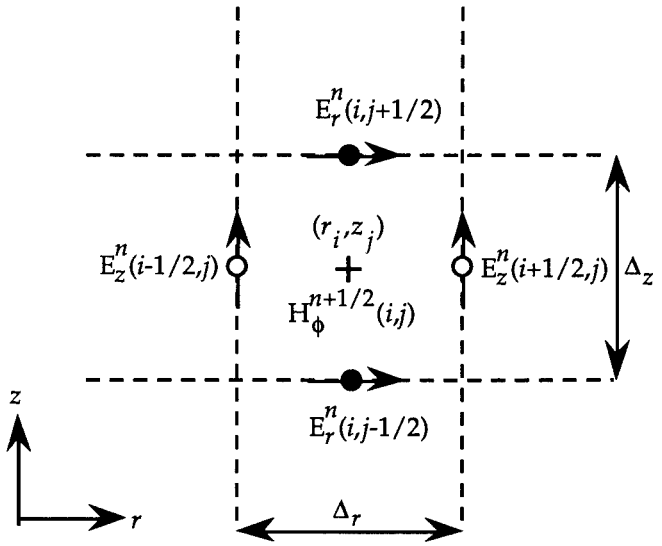

Figure 2.1: Interleaved electric and magnetic fields for FDTD grid cell.

To implement the Yee algorithm, the electric and magnetic field components are evaluated at interleaved spatial grid points and time steps [11], as shown in Figure 2.1. The derivatives in Equations 1-3 are replaced by the second-order accurate centred difference approximations, so that Maxwell's equations become

$$\begin{aligned} H_\phi^{n+1/2}(i,j) = H_\phi^{n-1/2}(i,j) &+ \frac{\Delta_t}{\mu_0\Delta_r}[E_z^n(i+1/2,j) - E_z^n(i-1/2,j)] - \frac{\Delta_t}{\mu_0\Delta_z}[E_r^n(i,j+1/2) \\ &- E_r^n(i,j-1/2)] \end{aligned} \tag{4}$$

$$E_r^{n+1}(i,j+1/2) = E_r^n(i,j+1/2) - \frac{\Delta_t}{\varepsilon\Delta_z}[H_\phi^{n+1/2}(i,j+1) - H_\phi^{n+1/2}(i,j)] \tag{5}$$

$$E_z^{n+1}(i+1/2,j) = E_r^n(i+1/2,j) + \frac{\Delta_t}{r_{i+1/2}\varepsilon\Delta_r}[r_{i+1}H_\phi^{n+1/2}(i+1,j) - [r_iH_\phi^{n+1/2}(i,j)] \qquad (6)$$

The field points $H_\phi^{n+1/2}(i, j)$, $E_r^{n+1}(i,j+1/2)$, and $E_z^{n+1}(i+1/2,j)$ are assigned to the grid cell (i,j) centred at (r_i,z_j)

For convergence, the mesh increments Δ_r, Δ_z, and Δ_t must satisfy the Courant-Friedrichs-Lewy condition

$$c\,\Delta_t \leq \sqrt{\Delta_r^2\,\Delta_z^2/(\Delta_r^2 + \Delta_z^2)}$$

where $c = 1/\sqrt{\varepsilon\mu_0}$ is the velocity of light.

2.2.2 Boundary Conditions

2.2.2.1 Edge Boundary Conditions

Practical considerations require that the mesh must be finite in its spatial dimensions as shown in Figure 2.2. From Equations 4-6, it is apparent that to simulate an unbounded space, a boundary condition is required at the edges of the mesh to specify the tangential component of the electric field. At $r = 0$ ($i = 0$), symmetry about the axis requires that

$$\frac{\partial E_z}{\partial r} = 0$$

Therefore

$$E_z^n(1/2,j) = E_z^n(-1/2,j)$$

and so

$$H_\phi^{n+1/2}(0, j) = H_\phi^{n-1/2}(0, j) - \frac{\Delta_t}{\mu_0\Delta_z}[E_r^n(0,j+1/2) - E_r^n(0,j-1/2)] \qquad (7)$$

Hence $E_z^n(1/2,j)$ is not required explicitly. Including the tangential electric field at the other three sides of the mesh is not so straightforward, and must be determined using absorbing boundary conditions in order to simulate an unbounded medium. Merewether [14] used the radiation condition for the electric field at a sufficiently large distance, R, from the centre of the antenna,

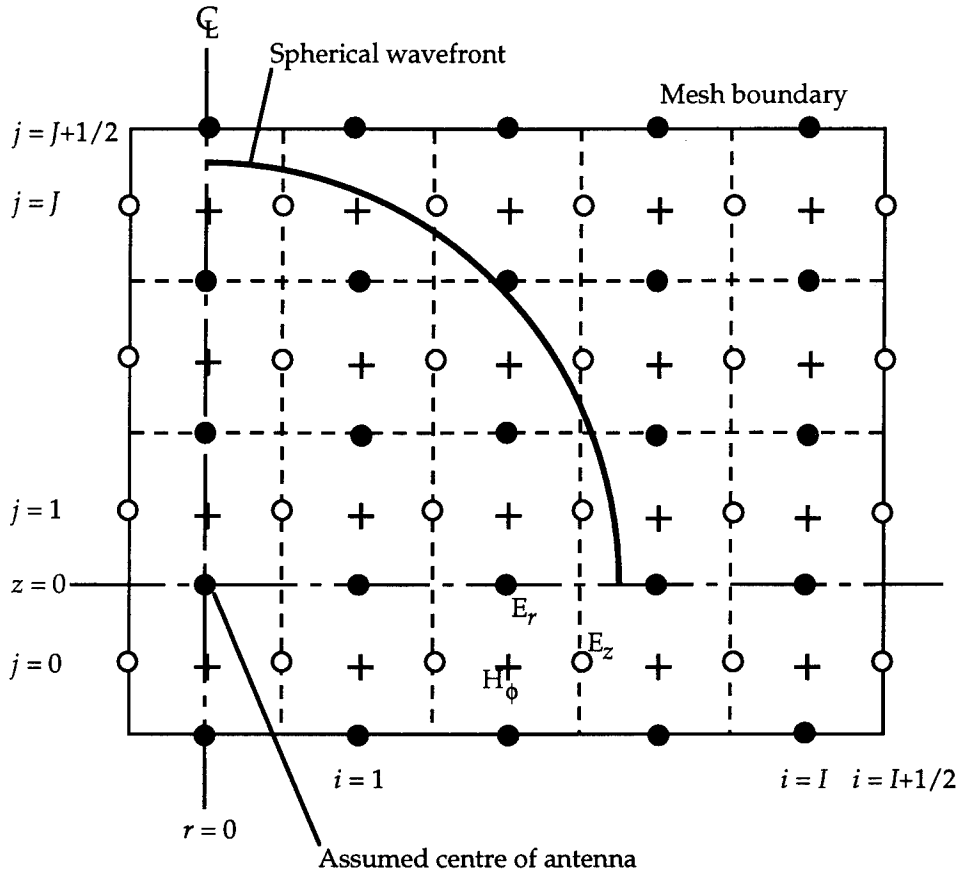

Figure 2.2: Truncated mesh in cylindrical geometry

$$E = \frac{f(t - R/c)}{R}$$

where f is some causal function, ie., $f(x) = 0$ for $x \leq 0$. This corresponds to an assumption that at a reasonable distance from the antenna the fields can be represented in terms of an outward travelling spherical wavefront. Consider E_r just beyond the upper axial limit of the mesh ($j = J$, $z = z_{max}$)

$$R(i,J+1/2)\, E_r^{n+1}(i,J+1/2) = f_r(t^{n+1} - R(i,J+1/2)/c)$$

$$= f_r(t^{n} - R(i,J-1/2)/c + \Delta_t\theta)$$

where

$$\theta = 1 - \frac{R(i,J+1) - R(i,J)}{c\,\Delta_t} \qquad ; \theta \le 1$$

and

$$R(i,j) = \sqrt{r_i^2 + (z_j - z_0)^2}$$

with z_0 the axial position of the geometric centre of the antenna.

Similarly, the field just inside the upper mesh boundary ($j = J$, $z = z_{max}$) is given by

$$R(i,J\text{-}1/2)\ E_r^n(i,J\text{-}1/2) = f_r(t^n - R(i,J\text{-}1/2)/c)$$

Therefore, it is possible to obtain $E_r^{n+1}(i,J+1/2)$ using parabolic interpolation between the elements of the time sequence of $E_r^n(i,J\text{-}1/2)$ as follows

$$\begin{aligned} E_r^{n+1}(i,J+1/2) = \frac{R(i,J+1/2)}{2R(i,J\text{-}1/2)} [&\theta(\theta\text{-}1)\ E_r^{n-1}(i,J\text{-}1/2) \\ &+ 2(1\text{-}\theta^2)\ E_r^n(i,J\text{-}1/2) + \theta(\theta+1)\ E_r^{n+1}(i,J\text{-}1/2)] \end{aligned} \tag{8}$$

Similarly, $E_r^{n+1}(i,\text{-}1/2)$ at the lower axial limit of the mesh ($j = 0$) is

$$\begin{aligned} E_r^{n+1}(i,\text{-}1/2) = \frac{R(i,\text{-}1/2)}{2R(i,1/2)} [&\theta(\theta\text{-}1)\ E_r^{n-1}(i,1/2) + 2(1\text{-}\theta^2)\ E_r^n(i,1/2) \\ &+ \theta(\theta+1)\ E_r^{n+1}(i,1/2)] \end{aligned} \tag{9}$$

$E_z^{n+1}(I+1/2,j)$ at the radial limit of the mesh ($i = I$) is calculated in a similar fashion starting from

$$\begin{aligned} R(I+1/2,j)\ E_z^{n+1}(I+1/2,j) &= f_z(t^{n+1} - R(I+1/2,j)/c) \\ &= f_z(t^n - R(I+1/2,j)/c + \Delta_t\theta) \end{aligned}$$

where

$$\theta = 1 - \frac{R(I+1/2,j) - R(I\text{-}1/2,j)}{c\,\Delta_t} \qquad ; \theta \le 1$$

Similarly

$$R(I\text{-}1/2,j)\, E_z^n(I\text{-}1/2,j) \;=\; f_z(t^n - R(I\text{-}1/2,j)/c)$$

Therefore, it is possible to calculate $E_z^{n+1}(I+1/2,j)$ at the side of the mesh using

$$E_z^{n+1}(I+1/2,j) \;=\; \frac{R(I\text{-}1/2,j)}{2\,R(I+1/2,j)}\,[\theta(\theta\text{-}1)\,E_z^{n-1}(I\text{-}1/2,j) + 2(1\text{-}\theta^2)\,E_z^n(I\text{-}1/2,j) + \theta(\theta+1)\,E_z^{n+1}(I\text{-}1/2,j)] \qquad (10)$$

Equations 7-10 are sufficient to determine the required tangential electric fields on the mesh boundary, provided that R is sufficiently large that the fields at the mesh boundary can be represented by spherical waves propagating outward from the centre of the antenna. Since R must be finite with a finite mesh size, Equations 7-10 constitute approximately absorbing boundary conditions.

2.2.2.2 Antenna Feed

Power is fed into the antenna through a coaxial line extending directly downward from the antenna feed point. The line dimensions are such that it can only support a TEM mode, which means that an exact absorbing boundary condition can be constructed inside the line. The impedance of the line is

$$Z_{\text{line}} \;=\; \frac{1}{2\pi}\sqrt{\frac{\mu_0}{\varepsilon}}\,\ln(b/a)$$

and is usually chosen to be 50 Ω. The TEM mode electric field in the line can be written as

$$E_r \;=\; h(t + z/c) + g(t - z/c) \qquad\qquad E_\phi \;=\; E_z \;=\; 0$$

where $g(t - z/c)$ represents the TEM wave travelling toward the antenna feed, and $h(t + z/c)$ represents the TEM wave reflected from the feed due to imperfect matching of the line to the antenna. This mismatch will also generate higher-order evanescent modes, so the coaxial line is extended a sufficient distance from the antenna feed point such that these evanescent modes have decayed to a negligible level before the boundary condition is imposed. A distance of $3(b\text{-}a)$ is ample for this purpose [12]. If the feed line is terminated with a match at $j = j_{\text{term}}$ corresponding to $z = z_{term}$, the electric field inside the line is given by

$$E_r^{n+1}(i,j_{\text{term}}\text{-}1/2) \;=\; h(t_{n+1}) + g(t_{n+1})$$

$$= h(t_n + \Delta_z/c - \Delta_t\theta) + g(t_n - \Delta_z/c - \Delta_t\theta)$$

So that

$$E_r^{n+1}(i,j_{\text{term}}-1/2) - g(t_n - \Delta_z/c - \Delta_t\theta) = h(t_n + \Delta_z/c - \Delta_t\theta)$$

$$= \xi^{n+1}(i,j_{\text{term}}-1/2)$$

where

$$\theta = 1 - \frac{\Delta_z}{c\Delta_t}$$

and $\xi(z,t)$ represents the reflected TEM wave. Proceeding in the same fashion as for the absorbing boundary conditions at the extremities of the mesh, the reflected field at the termination is

$$\xi^{n+1}(i,j_{\text{term}}-1/2) = \frac{1}{2}[\theta(\theta-1)\,\xi^{n-1}(i,j_{\text{term}}+1/2) + 2(1-\theta^2)\,\xi^{n}(i,j_{\text{term}}+1/2)$$

$$+ \theta(\theta+1)\,\xi_r^{n+1}(i,j_{\text{term}}+1/2)] \qquad (11)$$

To calculate $\xi^{n+1}(i,j)$, the incident field in the feed line is subtracted from the total field. The incident field in the coaxial line is given by

$$E_r^{\text{inc}}(t) = \frac{V_{\text{inc}}(t)}{\ln(b/a)r}$$

where $V_{\text{inc}}(t)$ is the user specified voltage applied to the antenna feed. A Gaussian pulse is commonly used, with

$$V_{\text{inc}}(t) = V_0 \exp\left[\frac{-t^2}{2\tau_p^2}\right]$$

where $\tau_p = 0.4246\, t_w$, where t_w is the FWHM pulse width.

Since only the TEM mode is supported in the feed, (11) constitutes an exactly absorbing boundary condition. The reflected voltage on the feed transmission line is calculated by averaging

$$V_{\text{refl}}(t) = \xi(i, j_{\text{term}}-1/2)\,\ln(b/a)\,r$$

over the radius of the line. The reflected voltage constitutes part of the output from the program. It is especially useful for identifying the nature of reflections from various parts of the antenna and for calculating antenna efficiency for a given excitation. The efficiency for a time domain antenna is the ratio of the transmitted to the excitation energy [15], and is calculated from

$$\eta = \frac{\int_0^\infty V_{inc}(t)^2\,dt - \int_0^\infty V_{refl}(t)^2\,dt}{\int_0^\infty V_{inc}(t)^2\,dt}$$

2.2.2.3 Conducting Surface Boundary Conditions

The implementation of conducting surface boundary conditions using the Yee formalism is particularly straightforward. The surface is approximated by a "staircase" as shown in Figure 2.3. Grid cells are filled if their centres lie within the conductor. E_r is set to zero at horizontal interfaces between filled and unfilled cells, and E_z is set to zero at vertical interfaces.

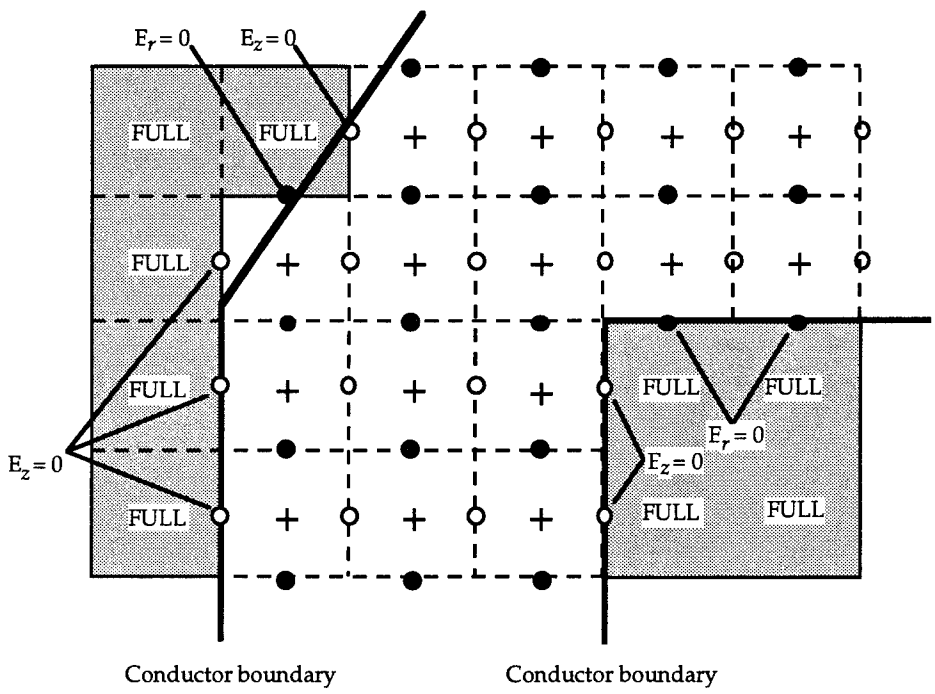

Figure 2.3: Staircased conducting boundaries

Although simple, this technique is known to introduce errors arising from the staircasing approximation when applied to surfaces which do not coincide with grid cell boundaries [16]. These errors are significant near regions of high field concentration such as antenna feed points. To more accurately model the arbitrarily shaped conducting boundaries of the antenna, the contour path formalism [17] described in Section 2.3 was adopted.

2.3 The Contour Path (CP) Approach

2.3.1 Mesh Equations

The contour path (CP) algorithm described by Jurgens *et al.*, [17] is based on Faraday's and Ampere's laws rather than Maxwell's equations

$$\oint_C \mathbf{E}.dl = -\frac{\partial}{\partial t}\iint_S \mu_0 \mathbf{H}.dS \tag{12}$$

$$\oint_C \mathbf{H}.dl = \frac{\partial}{\partial t}\iint_S \varepsilon \mathbf{E}.dS \tag{13}$$

where the contour C encloses the surface S. The contours used for Equations 12 and 13 intersect each other's enclosed surface in a manner resembling the links of a chain, as shown in Figure 2.4.

Equations 12 and 13 are implemented by defining the electric and magnetic field values at interleaved grids in the *r-z* plane as discussed in Section 2.2. As for the Yee method, a centred finite difference approximation is used for the time derivatives. To evaluate the surface integral in Equation 12, assume that H_ϕ is constant over a grid patch and equal to the value at the centre of the patch as shown in Figure 2.4. In addition, E_r and E_z are assumed to have no variation along the individual sides of the patch. For the cell centred at (r_i, z_j)

$$-\frac{\partial}{\partial t}\iint_S \mu_0 \mathbf{H}(r_i, z_j).dS = -\mu_0 \frac{\partial}{\partial t}\int_{z_{j-1/2}}^{z_{j+1/2}}\int_{r_{i-1/2}}^{r_{i+1/2}} H_\phi(i, j)\, dr\, dz$$

$$= -\frac{\mu_0}{\Delta_t}\left(H_\phi^{n+1/2}(i, j) - H_\phi^{n-1/2}(i, j)\right) A_{cell}$$

where A_{cell} is the area of the grid cell in the r-z plane. From Figure 2.4, the contour integral is calculated using

$$\oint_C \mathbf{E}.dl = E_z^n(i+1/2,j)\, l_{right} - E_z^n(i-1/2,j)\, l_{left} + E_r^n(i,j-1/2)\, l_{low} - E_r^n(i,j+1/2)\, l_{up}$$

where l_{right} and l_{left} are lengths of the left and right sides of the cell, and l_{low} and l_{up} are the lengths of the upper and lower sides of the cell. Therefore

$$H_\phi^{n+1/2}(i,j) = H_\phi^{n-1/2}(i,j) + \frac{\Delta_t}{\mu_0 A_{cell}} \left(E_z^n(i+1/2,j)\, l_{right} - E_z^n(i-1/2,j)\, l_{left} + E_r^n(i,j-1/2)\, l_{low} - E_r^n(i,j+1/2)\, l_{up}\right) \quad (14)$$

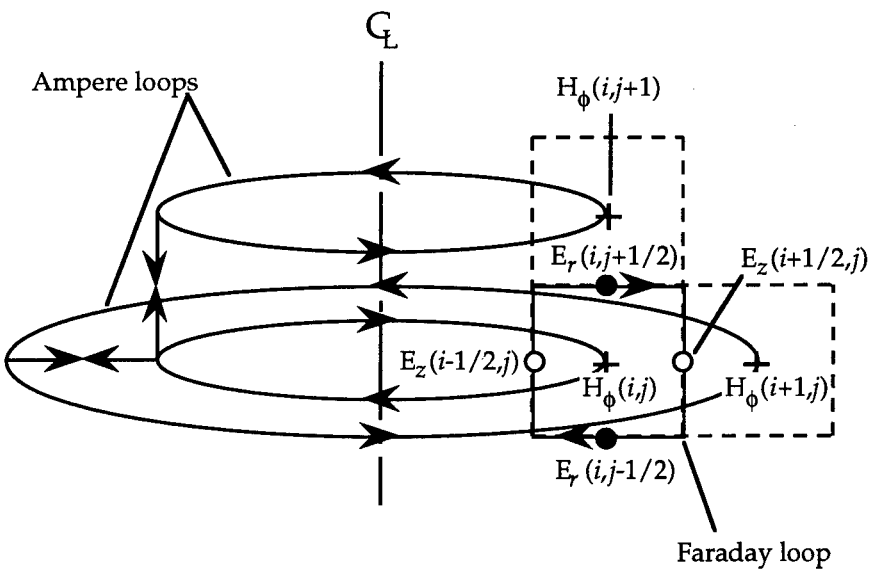

Figure 2.4: Ampere and Faraday contour geometry for Contour Path technique

For a simple rectangular grid cell, $A_{cell} = \Delta_r\Delta_z$, $l_{up} = l_{low} = \Delta_r$, and $l_{left} = l_{right} = \Delta_z$. Equation 14 then reduces to Equation 4 as derived from the Yee approach.

Since there is azimuthal symmetry, $E_r^n(i,j+1/2)$ is found from Equation 13 by integrating over and around the Ampere loop shown in Figure 2.4. Note that only H_ϕ contributes to the line integral since the contributions from the segment connecting the two loops cancel each other. It follows that

$$\frac{\partial}{\partial t}\iint_S \varepsilon \mathbf{E}.dS = \frac{\partial}{\partial t}\int_{z_j}^{z_{j+1}}\int_0^{2\pi} \varepsilon E_r(i,j+1/2)\,(r_i d\phi)dz$$

$$= \frac{\varepsilon_0}{\Delta_t}(E_r^{n+1}(i,j+1/2) - E_r^{n}(i,j+1/2)\; 2\pi r_i$$

$$(\varepsilon_r(i,j+1)\; l_{up}^{diel} + \varepsilon_r(i,j)\; l_{low}^{diel})$$

where l_{up}^{diel} and l_{low}^{diel} are the distances from a possible dielectric interface to points (r_i, z_{j+1}) and (r_i, z_j), respectively, and $\varepsilon_r(i, j)$ is the relative dielectric constant at mesh point (r_i, z_j). Note that only a horizontal dielectric interface is allowed at points $(r_i, z_{j+1/2})$ where E_r is calculated. The contour integral from Equation 8 is

$$\oint_C \mathbf{H}.dl = -2\pi r_i\,(H_\phi^{n+1/2}(i,j+1) - H_\phi^{n+1/2}(i,j))$$

Therefore

$$E_r^{n+1}(i,j+1/2) = E_r^{n}(i,j+1/2) - \frac{\Delta_t}{\varepsilon_0}\frac{H_\phi^{n+1/2}(i,j+1) - H_\phi^{n+1/2}(i,j)}{\varepsilon_r(i,j+1)\; l_{up}^{diel} + \varepsilon_r(i,j)\; l_{low}^{diel}} \tag{15}$$

For the simple case of uniform dielectric constant and $l_{low}^{diel} + l_{up}^{diel} = \Delta_z$, Equation 15 reduces to Equation 5 as for the Yee formalism.

$E_z^{n}(i,j+1/2)$ was calculated in a similar fashion. The surface integral is

$$\frac{\partial}{\partial t}\iint_S \varepsilon \mathbf{E}.dS = \frac{\partial}{\partial t}\int_{r_i}^{r_{i+1}}\int_0^{2\pi} \varepsilon E_z(i+1/2,j)\,(r_i d\phi)dr$$

$$= \frac{\varepsilon_0}{\Delta_t}(E_z^{n+1}(i+1/2,j) - E_z^{n}(i+1/2,j)\; 2\pi$$

$$(\varepsilon_r(i+1,j)\, r_{i+1} l^{diel}_{right} + r_i\, \varepsilon_r(i,j)\, l^{diel}_{left})$$

where l^{diel}_{right} and l^{diel}_{left} are the lengths from the dielectric interface to points (r_{i+1}, z_j) and (r_i, z_j), respectively. Note that only a vertical dielectric interface is allowed at points $(r_{i+1/2}, z_j)$ where E_z is calculated. The corresponding contour integral is

$$\oint_C \mathbf{H}.dl \quad = \quad 2\pi(r_{i+1}\, H_\phi^{n+1/2}(i+1j) - r_i\, H_\phi^{n+1/2}(i,j))$$

Therefore

$$E_z^{n+1}(i+1/2,j) = E_z^n(i+1/2j) - \frac{\Delta_t}{\varepsilon_0} \frac{r_{i+1}\, H_\phi^{n+1/2}(i+1j) - r_i\, H_\phi^{n+1/2}(i,j)}{\varepsilon_r(i+1,j)\, r_{i+1} l^{diel}_{right} + \varepsilon_r\, r_i\, (i,j)\, l^{diel}_{left}} \tag{16}$$

For the simple case of uniform dielectric constant and $l^{diel}_{right} + l^{diel}_{left} = \Delta_r$, Equation 16 reduces to Equation 6 from the Yee formalism.

It is clear that for simple rectangular grid cells, the mesh equations derived using the contour path approach are exactly the same as those derived using the Yee method. However, it is near conducting boundaries that the contour path method is most useful. If one of the sides of the cell coincides with the conducting surface, then the tangential component of the electric field along that side disappears. It does not matter that the cell is no longer rectangular as the shape of the cell is not fundamentally constrained in the contour path approach as it is in the Yee formalism. A thorough discussion of cell deformation near conducting surfaces is presented in the next section.

2.3.2 Boundary Conditions

The boundary conditions at the extremities of the mesh which were derived for the Yee formalism are equally valid for the contour path method, so this section will deal exclusively with boundary conditions near conductors. For the grid cells adjacent to conducting surfaces, the Faraday contours used for the integration in Equation 12 are deformed so as to conform to the surface of the conductor. Ampere contours are not deformed, and E_r and E_z values which require using Ampere contours which cross media boundaries are not used. For this reason, only the calculation of H_ϕ values is affected by the presence of a conductor. The calculation of E_r and E_z values is essentially identical to the Yee method.

2.3.2.1 Horizontal Cell Deformation

For the case where a conducting boundary lies to the left of a grid cell, and the slope of the conductor is greater than Δ_z/Δ_r with respect to the horizontal as shown in Figure 2.5, then H_ϕ is calculated from

$$H_\phi^{n+1/2}(i,j) = H_\phi^{n-1/2}(i,j) + \frac{\Delta_t}{\mu_0 A_{cell}} \left(E_z^n(i+1/2,j)\, l_{right} + E_r^n(i,j-1/2)\, l_{low} - E_r^n(i,j+1/2)\, l_{up}\right)$$

If the centre of the cell immediately above located at (r_i, z_{j+1}) is inside the conductor, then the Ampere contour used to calculate $E_r^n(i,j+1/2)$ is discarded and the nearest neighbour value on the right is used, so that

$$H_\phi^{n+1/2}(i,j) = H_\phi^{n-1/2}(i,j) + \frac{\Delta_t}{\mu_0 A_{cell}} \left(E_z^n(i+1/2,j)\, l_{right} + E_r^n(i,j-1/2)\, l_{low} - E_r^n(i+1,j+1/2)\, l_{up}\right)$$

Similarly, if the centre of the cell immediately below located at (r_i, z_{j-1}) is inside the conductor, then

$$H_\phi^{n+1/2}(i,j) = H_\phi^{n-1/2}(i,j) + \frac{\Delta_t}{\mu_0 A_{cell}} \left(E_z^n(i+1/2,j)\, l_{right} + E_r^n(i+1,j-1/2)\, l_{low} - E_r^n(i,j+1/2)\, l_{up}\right)$$

If the conducting surface is to the right of the cell, the treatment is similar except that the electric field on the right side of the cell is set to zero. Nearest neighbour values on the left are used to interpolate $E_r^n(i,j+1/2)$ and $E_r^n(i,j-1/2)$ where Ampere contours are not available. For this instance

$$H_\phi^{n+1/2}(i,j) = H_\phi^{n-1/2}(i,j) + \frac{\Delta_t}{\mu_0 A_{cell}} \left(E_z^n(i-1/2,j)\, l_{left} + E_r^n(i,j-1/2)\, l_{low} - E_r^n(i,j+1/2)\, l_{up}\right)$$

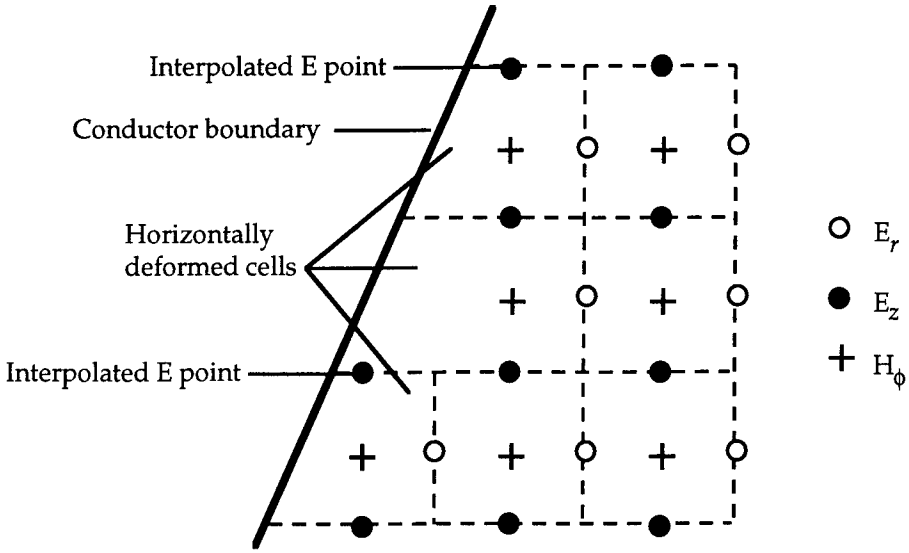

Figure 2.5 Horizontal cell deformation near conducting surface

2.3.2.1 Vertical Cell Deformation

If the slope of the conducting boundary is less than Δ_z/Δ_r relative to the horizontal, it would become possible for the vertical cell sides to be truncated, complicating the situation. In addition, inaccuracy could be introduced if the electric field values are held constant over unnecessarily long upper and lower cell sides. For these reasons, it is better to deform the grid cells vertically in this instance. For the case where a conducting boundary lies just above a grid cell as shown in Figure 2.6, then H_ϕ is calculated from

$$H_\phi^{n+1/2}(i,j) = H_\phi^{n-1/2}(i,j) + \frac{\Delta_t}{\mu_0 A_{cell}} \left(E_z^n(i+1/2,j)\, l_{right} - E_z^n(i-1/2,j)\, l_{left} + E_r^n(i,j-1/2)\, l_{low}\right)$$

If the centre of the cell immediately to the right at (r_{i+1}, z_j) is inside the conductor, then the Ampere contour used to calculate $E_z^n(i+1/2,j)$ is discarded and the nearest neighbour value from below is used, so that

$$H_\phi^{n+1/2}(i,j) = H_\phi^{n-1/2}(i,j) + \frac{\Delta_t}{\mu_0 A_{cell}} \left(E_z^n(i+1/2,j-1)\, l_{right} - E_z^n(i-1/2,j)\, l_{left} + E_r^n(i,j-1/2)\, l_{low}\right)$$

Similarly, if the centre of the cell immediately to the left at (r_{i-1}, z_j) is inside the conductor, then

$$H_\phi^{n+1/2}(i,j) = H_\phi^{n-1/2}(i,j) + \frac{\Delta_t}{\mu_0 A_{cell}} \left(E_z^n(i+1/2,j)\, l_{right} - E_z^n(i-1/2,j-1)\, l_{left} + E_r^n(i+1,j-1/2)\, l_{low}\right)$$

If the conducting surface is below the grid cell the treatment is similar, except that the electric field on the bottom of the cell is set to zero. Nearest neighbour values from above are used to interpolate $E_z^n(i+1/2,j)$ and $E_z^n(i-1/2,j)$ where Ampere contours are not available. For this situation

$$H_\phi^{n+1/2}(i,j) = H_\phi^{n-1/2}(i,j) + \frac{\Delta_t}{\mu_0 A_{cell}} \left(E_z^n(i+1/2,j)\, l_{right} - E_z^n(i+1/2,j)\, l_{left} - E_r^n(i,j+1/2)\, l_{up}\right)$$

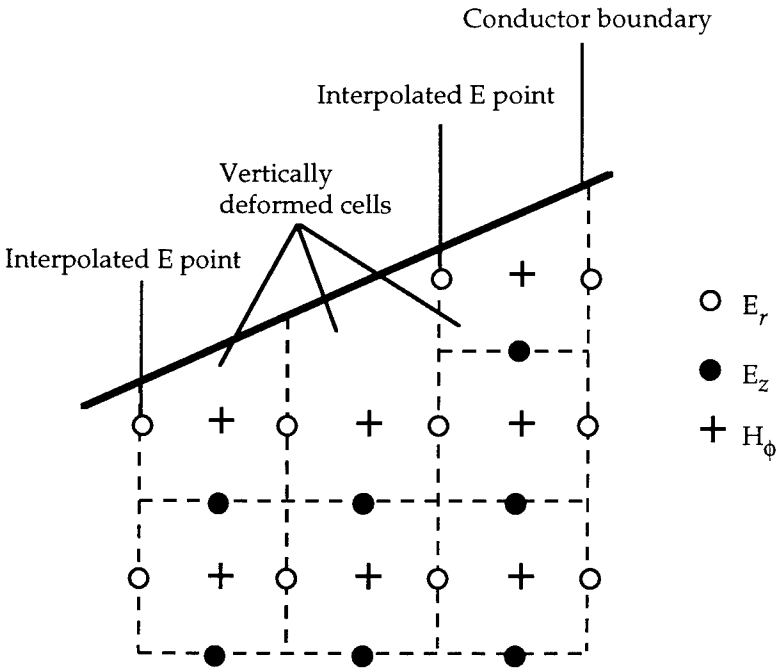

Figure 2.6: Vertical cell deformation near conducting surface

2.5 Far Field Calculation

The technique developed in [18] was used to calculate the electric field in the far zone from the fields close to the object which are determined using the FDTD method. From [19], the radiation vectors **N** and **L** over a closed surface S' with local surface normal $\hat{\mathbf{n}}$ are defined in the frequency domain to be

$$\mathbf{N}(k) = \int_{S'} \hat{\mathbf{n}} \times \mathbf{H}(\mathbf{R}', k) \exp(-jk\mathbf{R}'.\hat{\mathbf{R}})\, dS'$$

$$\mathbf{L}(k) = -\int_{S'} \hat{\mathbf{n}} \times \mathbf{E}(\mathbf{R}', k) \exp(-jk\mathbf{R}'.\hat{\mathbf{R}})\, dS'$$

where k = $2\pi f/c$, **R** is the vector from the centre of the antenna to the far-field point and **R**' is the vector to the point on the surface S' enclosing the antenna. Using spherical coordinates with the origin located at the centre of the antenna, the only electric field components which do not decrease faster than 1/R are

$$E_\theta(k) = \zeta_0 H_\phi(k) = -j\frac{\exp(-jkR)}{2\lambda R}(\zeta_0 N_\theta + L_\phi)$$

$$E_\phi(k) = -\zeta_0 H_\theta(k) = j\frac{\exp(-jkR)}{2\lambda R}(-\zeta_0 N_\phi + L_\theta)$$

where ζ_0 is the impedance of free space. Following [18], define

$$\mathbf{W}(k) = j\frac{\exp(-jkR)}{2\lambda R}\mathbf{N}$$

$$\mathbf{U}(k) = j\frac{\exp(-jkR)}{2\lambda R}\mathbf{L}$$

Taking the inverse Fourier transform of **W** and **U** leads to

$$\mathbf{w}(t) = \frac{1}{4\pi Rc}\frac{\partial}{\partial t'}\int_{S'} \hat{\mathbf{n}} \times \mathbf{H}(\mathbf{R}', t')\, dS'$$

$$\mathbf{u}(t) = -\frac{1}{4\pi Rc}\frac{\partial}{\partial t'}\int_{S'} \hat{\mathbf{n}} \times \mathbf{E}(\mathbf{R}', t')\, dS'$$

where $t' = t - |\mathbf{R} - \mathbf{R}'|/c$ is the retarded time. The time-domain electric field in the far zone is calculated from

$$E_\theta(\mathbf{R}, t) = -(\zeta_0 w_\theta + u_\phi)$$

$$= \frac{1}{4\pi Rc} \iint_{S'} \left[-\zeta_0 \frac{\partial}{\partial t'} [\hat{\mathbf{n}} \times \mathbf{H}(\mathbf{R}', t')]_\theta + \frac{\partial}{\partial t'} [\hat{\mathbf{n}} \times \mathbf{E}(\mathbf{R}', t')]_\phi \right] dS' \tag{17}$$

$$E_\phi(\mathbf{R}, t) = -\zeta_0 w_\phi + u_\theta$$

$$= \frac{1}{4\pi Rc} \iint_{S'} \left[-\zeta_0 \frac{\partial}{\partial t'} [\hat{\mathbf{n}} \times \mathbf{H}(\mathbf{R}', t')]_\phi - \frac{\partial}{\partial t'} [\hat{\mathbf{n}} \times \mathbf{E}(\mathbf{R}', t')]_\theta \right] dS' \tag{18}$$

Equations 17 and 18 can be combined and expressed as

$$\mathbf{E}(\mathbf{R}, t) = \frac{-\zeta_0}{4\pi Rc}$$

$$\left[\int_{S'} \frac{\partial}{\partial t'} [\hat{\mathbf{n}} \times \mathbf{H}(\mathbf{R}', t')]\, dS' + \frac{1}{\zeta_0} \int_{S'} \hat{\mathbf{R}} \times \frac{\partial}{\partial t'} [\hat{\mathbf{n}} \times \mathbf{E}(\mathbf{R}', t')]\, dS' \right]$$

$$= \frac{\mu_0}{4\pi R} \Big[\int_{S'} \hat{\mathbf{R}} \times \hat{\mathbf{R}} \times \frac{\partial}{\partial t'} [\hat{\mathbf{n}} \times \mathbf{H}(\mathbf{R}', t')]\, dS'$$

$$- \frac{1}{\zeta_0} \int_{S'} \hat{\mathbf{R}} \times \frac{\partial}{\partial t'} [\hat{\mathbf{n}} \times \mathbf{E}(\mathbf{R}', t')]\, dS' \Big] \tag{19}$$

Equation 19 is identical to Equation 7 presented in [12]. For convenience, a cylindrical surface was used to enclose the antenna. The side of the cylinder extended from the ground plane at $j = j_{gp}$ up to $j = j_{top}$. The radius of the cylinder was r_{side}. There are contributions to the surface integral in Equation 17 and 18 from both the side and top of the cylindrical surface. Converting from cylindrical to cartesian coordinates, for the side of the surface

$$\hat{\mathbf{n}} \times \mathbf{H}(\mathbf{R}', t') = H_\phi(\mathbf{R}', t')\,\hat{\mathbf{z}} \quad \text{and} \quad \hat{\mathbf{n}} \times \mathbf{E}(\mathbf{R}', t') = -E_z(\mathbf{R}', t')\,\hat{\boldsymbol{\phi}}$$

$$= E_z(\mathbf{R}', t')\,[\sin\phi'\,\hat{\mathbf{x}} - \cos\phi'\,\hat{\mathbf{y}}]$$

and from the top of the surface

$$\hat{\mathbf{n}} \times \mathbf{H}(\mathbf{R}', t') = -H_\phi(\mathbf{R}', t')\,\hat{\mathbf{r}} \quad \text{and} \quad \hat{\mathbf{n}} \times \mathbf{E}(\mathbf{R}', t') = E_z(\mathbf{R}', t')\,\hat{\boldsymbol{\phi}}$$

$$= H_\phi(\mathbf{R}', t')\,[-\cos\phi'\,\hat{\mathbf{x}} - \sin\phi'\,\hat{\mathbf{y}}]$$

$$= E_r(\mathbf{R}', t')\,[-\sin\phi'\,\hat{\mathbf{x}} + \cos\phi'\,\hat{\mathbf{y}}]$$

At the far zone point where ϕ is set arbitrarily to zero since $\frac{\partial}{\partial\phi} = 0$, then $\hat{\mathbf{x}}$, $\hat{\mathbf{y}}$, and $\hat{\mathbf{z}}$ can be expressed in terms of $\hat{\mathbf{R}}$, $\hat{\boldsymbol{\theta}}$, and $\hat{\boldsymbol{\phi}}$ at the far zone point $(R, \theta, 0)$ as follows

$$\hat{\mathbf{x}} = \hat{\mathbf{R}}\sin\theta + \hat{\boldsymbol{\theta}}\cos\theta$$

$$\hat{\mathbf{y}} = \hat{\boldsymbol{\phi}}$$

$$\hat{\mathbf{z}} = \hat{\mathbf{R}}\cos\theta - \hat{\boldsymbol{\theta}}\sin\theta$$

So at the side of the cylindrical surface

$$\hat{\mathbf{n}} \times \mathbf{H}(\mathbf{R}', t') = H_\phi(\mathbf{R}', t')\,[\cos\theta\,\hat{\mathbf{R}} - \sin\theta\,\hat{\boldsymbol{\theta}}]$$

and hence

$$\hat{\mathbf{R}} \times \hat{\mathbf{R}} \times \hat{\mathbf{n}} \times \mathbf{H}(\mathbf{R}', t') = H_\phi(\mathbf{R}', t')\sin\theta\;\hat{\boldsymbol{\theta}}$$

Also

$$\hat{\mathbf{n}} \times \mathbf{E}(\mathbf{R}', t') = E_z(\mathbf{R}', t')\,[\sin\theta\sin\phi'\,\hat{\mathbf{R}} + \cos\theta\sin\phi'\,\hat{\boldsymbol{\theta}} - \cos\phi'\,\hat{\boldsymbol{\phi}}]$$

which leads to

$$\hat{\mathbf{R}} \times \hat{\mathbf{n}} \times \mathbf{E}(\mathbf{R}', t') = E_z(\mathbf{R}', t')\,[\cos\phi'\,\hat{\boldsymbol{\theta}} + \cos\theta\sin\phi'\,\hat{\boldsymbol{\phi}}]$$

The contribution to the far zone electric field from the side of the cylindrical surface is

$$\mathbf{E}^{side}(\mathbf{R}, t) = \frac{\mu_0}{4\pi R}\Big[\int_{side} \hat{\mathbf{R}} \times \hat{\mathbf{R}} \times \frac{\partial}{\partial t'}[\hat{\mathbf{n}} \times \mathbf{H}(\mathbf{R}', t')]\, dS'$$

$$- \frac{1}{\zeta_0}\int_{side} \hat{\mathbf{R}} \times \frac{\partial}{\partial t'}[\hat{\mathbf{n}} \times \mathbf{E}(\mathbf{R}', t')]\, dS'\Big]$$

$$= \frac{\mu_0 r_{side}}{4\pi R}\Big[\int_0^{2\pi} \sin\theta \int_{z_{gp}}^{z_{top}} \frac{\partial}{\partial t'} \mathrm{H}_\phi(r_{side}, z', t')\, dz'\, d\phi'\, \hat{\theta}$$

$$- \frac{1}{\zeta_0}\int_0^{2\pi} \int_{z_{gp}}^{z_{top}} \frac{\partial}{\partial t'} \mathrm{E}_z(\mathbf{R}', t')\, dz'\, [\cos\phi'\, \hat{\theta} + \cos\theta \sin\phi'\, \hat{\phi}]\, d\phi'\, \Big]$$

$$= \frac{\mu_0 r_{side}}{4\pi R}\Big[\sin\theta \int_0^{2\pi} \int_{z_{gp}}^{z_{top}} \frac{\partial}{\partial t'} \mathrm{H}_\phi(r_{side}, z', t')\, dz'\, d\phi'\, \hat{\theta}$$

$$- \frac{1}{\zeta_0}\int_0^{2\pi} \int_{z_{gp}}^{z_{top}} \frac{\partial}{\partial t'} \mathrm{E}_z(\mathbf{R}', t')\, dz' \cos\phi'\, d\phi'\Big]\, \hat{\theta} \qquad (20)$$

since $\mathrm{E}_z(\mathbf{R}', t')$ is an even function of ϕ', as can be seen from

$$t' = t - \frac{|\mathbf{R} - \mathbf{R}'|}{c}$$

$$= t - \frac{\sqrt{(\mathrm{R}\sin\theta - r_{side}\cos\phi')^2 + r_{side}^2\sin^2\phi' + (\mathrm{R}\cos\theta - z')^2}}{c}$$

$$\approx t - \mathrm{R}/c - \frac{r_{side}\sin\theta\cos\phi' + z'\cos\theta}{c}$$

in the far field region.

When evaluating Equation 18 the 1/R dependence is suppressed. To calculate $\mathbf{E}^{side}(\mathbf{R}, t)$, $\mathrm{H}_\phi(r_{side}, z', t')$ and $\mathrm{E}_z(\mathbf{R}', t')$ are required for times $t = n\Delta_t$. Since **E** and **H** on the surface are only calculated at times 0, Δ_t, $2\Delta_t$, ..., then $\mathbf{E}^{side}(\mathbf{R}, t)$ cannot be evaluated for any given t. Let t'_{jmn} be defined as

$$t'_{jmn} = n\,\Delta_t - \frac{r_{side}\sin\theta\cos\phi'_m + z'_j\cos\theta}{c}$$

where the R/c time delay has been ignored. Consider the first integral

$$I_H(\hat{\mathbf{R}}t) = \int_0^{2\pi}\int_{z_{gp}}^{z_{top}} \frac{\partial}{\partial t'}\mathrm{H}_\phi(r_{side}, z', t')\,dz'\,d\phi'$$

Using sum approximations for the ϕ and z integrals leads to

$$I_H(\hat{\mathbf{R}}t_k) = \Delta_\phi\,\Delta_z \sum_{m=0}^{2\pi}\sum_{j=j_{gp}}^{j_{top}} \frac{\partial}{\partial t'}\mathrm{H}_\phi(i_{side}, j, t'_{jmn})$$

where the time t_k is defined using

$$k = \mathrm{int}\,(t_{jmn}/\Delta_t)$$

$$t_k = k\,\Delta_t$$

Therefore, the field at a given point on the side on the cylindrical surface $z = z_j$, $\phi = \phi_m$, at time $t = n\,\Delta_t$ contributes to the far field at a given **R** in the kth

retarded time "bin" corresponding to time t_k. The integral is evaluated by summing the contributions over all times from all points on the surface for each t_k bin. All of the required integrals were evaluated in this fashion.

At the top of the cylindrical surface

$$\hat{\mathbf{n}} \times \mathbf{H}(\mathbf{R}', t') = -\mathrm{H}_{\phi}(\mathbf{R}', t') [\sin\theta \cos\phi' \hat{\mathbf{R}} + \cos\theta \cos\phi' \hat{\theta} + \sin\phi' \hat{\phi}]$$

and hence

$$\hat{\mathbf{R}} \times \hat{\mathbf{R}} \times \hat{\mathbf{n}} \times \mathbf{H}(\mathbf{R}', t') = \mathrm{H}_{\phi}(\mathbf{R}', t') [\cos\theta \cos\phi' \hat{\theta} + \sin\phi' \hat{\phi}]$$

Also

$$\hat{\mathbf{n}} \times \mathbf{E}(\mathbf{R}', t') = \mathrm{E}_r(\mathbf{R}', t') [-\sin\theta \sin\phi' \hat{\mathbf{R}} - \cos\theta \sin\phi' \hat{\theta} + \cos\phi' \hat{\phi}]$$

which leads to

$$\hat{\mathbf{R}} \times \hat{\mathbf{n}} \times \mathbf{E}(\mathbf{R}', t') = -\mathrm{E}_r(\mathbf{R}', t') [\cos\phi' \hat{\theta} + \cos\theta \sin\phi' \hat{\phi}]$$

The contribution to the far zone electric field from the top of the cylindrical surface is therefore

$$\mathbf{E}^{top}(\mathbf{R}, t) = \frac{\mu_0}{4\pi R} [\int_{top} \hat{\mathbf{R}} \times \hat{\mathbf{R}} \times \frac{\partial}{\partial t'} [\hat{\mathbf{n}} \times \mathbf{H}(\mathbf{R}', t')] \, dS'$$

$$- \frac{1}{\zeta_0} \int_{top} \hat{\mathbf{R}} \times \frac{\partial}{\partial t'} [\hat{\mathbf{n}} \times \mathbf{E}(\mathbf{R}', t')] \, dS']$$

$$= \frac{\mu_0}{4\pi R}$$

$$[\int_0^{2\pi} \int_0^{r_{side}} r' \frac{\partial}{\partial t'} \mathrm{H}_{\phi}(r', z_{top}, t') \, dr' \, [\cos\theta \cos\phi' \hat{\theta} + \sin\phi' \hat{\phi}] \, d\phi'$$

$$+ \frac{1}{\zeta_0} \int_0^{2\pi} \int_0^{r_{side}} r' \frac{\partial}{\partial t'} \mathrm{E}_r(\mathbf{R}', t')\, dz' \, [\cos\phi' \, \hat{\theta} + \cos\theta \sin\phi' \, \hat{\phi}] \, d\phi' \,]$$

$$= \frac{\mu_0}{4\pi R} [\cos\theta \int_0^{2\pi} \int_0^{r_{side}} r' \frac{\partial}{\partial t'} \mathrm{H}_\phi(r', z_{top}, t')\, dr' \cos\phi' \, d\phi' \, \hat{\theta}$$

$$+ \frac{1}{\zeta_0} \int_0^{2\pi} \int_0^{r_{side}} r' \frac{\partial}{\partial t'} \mathrm{E}_r(\mathbf{R}', t')\, dr' \cos\phi' \, d\phi' \, \hat{\theta} \,] \qquad (21)$$

since $\mathrm{E}_r(\mathbf{R}', t')$ is an even function of ϕ', as can be seen from

$$t' = t - \frac{|\mathbf{R} - \mathbf{R}'|}{c}$$

$$= t - \frac{\sqrt{(\mathrm{R}\sin\theta - r'\cos\phi')^2 + r'^2 \sin^2\phi' + (\mathrm{R}\cos\theta - z_{top})^2}}{c}$$

$$\approx t - \mathrm{R}/c - \frac{r'\sin\theta\cos\phi' + z_{top}\cos\theta}{c}$$

As for Equation 20, when evaluating Equation 21 the 1/R dependence is suppressed. Let t'_{imn} be defined as

$$t'_{imn} = n\,\Delta_t - \frac{r'_i \sin\theta \cos\phi'_m + z_{top}\cos\theta}{c}$$

where the R/c time delay has been ignored. Consider the first integral

$$I(\hat{\mathrm{R}}t) = \int_0^{r_{side}} r' \frac{\partial}{\partial t'} \mathrm{H}_\phi(r', z_{top}, t')\, dr' \cos\phi'\, d\phi')$$

Using sum approximations for the ϕ and z integrals leads to

$$I(\hat{\mathrm{R}}t_k) = \Delta_\phi \Delta_r \sum_{m=0}^{2\pi} \sum_{i=0}^{i_{side}} \cos(m\Delta_\phi)\, r_i \frac{\partial}{\partial t'} \mathrm{H}_\phi(i, j_{top}, t'_{imn})$$

where the time t_k is defined using

$$k = \mathrm{int}\,(t_{imn}/\Delta_t)$$

$$t_k = k\,\Delta_t$$

Note that for antennas mounted on an infinite ground plane, the fields from the antenna image below the ground plane must be included in the surface integration to simulate the effect of the ground plane.

From the expressions derived in this section, the electric field in the far field region at an angle θ from the antenna at a given time can be calculated from the FDTD field quantities at previous times on a cylindrical surface surrounding the antenna. The far field calculation is central to obtaining predictions of the transmit and receive responses of the antenna.

2.6 Energy Calculation

To calculate the efficiency of the antenna for a specified excitation voltage, it is necessary to integrate the power radiated from the antenna, and compare it to the integrated input power. By checking the energy reflected from the antenna back through the feed, conservation of energy can be used to test the validity of the calculation. Following [15], the net power transmitted by the antenna, E_{trans}, is given by

$$\mathrm{E}_{trans} = \int_0^{\infty} \frac{\mathrm{V}_{in}^2 - \mathrm{V}_{refl}^2}{\mathrm{Z}_{\mathrm{coax}}}\, dt$$

where V_{in} is the applied voltage at the feed, V_{refl} is the voltage reflected from the antenna back through the feed, and $\mathrm{Z}_{\mathrm{coax}}$ is the impedance of the coaxial feed line. The efficiency of the antenna can be calculated from

$$\eta = \frac{\displaystyle\int_0^\infty \frac{V_{in}^2 - V_{refl}^2}{Z_{coax}}\,dt}{\displaystyle\int_0^\infty \frac{V_{in}^2}{Z_{coax}}\,dt}$$

The power radiated through the same cylindrical surface used for the far field calculation was determined using

$$P_{rad}^{top}(t) = \int_0^{r_{side}} 2\pi r\, E_r(r,z,t)\, H_\phi(r,z,t)\, dr$$

over the top of the cylindrical surface from $r = 0$ to $r = r_{side}$, and

$$P_{rad}^{side}(t) = -\int_{z_{gp}}^{z_{top}} 2\pi r\, E_z(r,z,t)\, H_\phi(r,z,t)\, dz$$

over the side of the surface from the ground plane at $z = z_{gp}$ to $z = z_{top}$. The electric fields E_r and E_z were linearly interpolated using the values at the edge of the grid cells to find their values at the centre of the cells where H_ϕ was evaluated. A linear time interpolation was also needed because the H_ϕ values are calculated at time points $(n+1/2)\Delta_t$, as opposed to $n\Delta_t$ for E_r and E_z. The total energy radiated by the antenna, E_{rad}, is therefore

$$E_{rad} = \int_0^\infty P_{rad}^{top}(t) + P_{rad}^{side}(t)\, dt$$

For a lossless antenna, E_{rad} should equal E_{trans}. The ratio E_{rad}/E_{trans} was calculated to assess the validity of the FDTD calculation, with 1 being the nominal result provided a sufficiently long time span is utilised.

2.7 Coarse Outer Mesh

In order for the absorbing boundary conditions to be effective, the mesh limits were required to be some distance from the antenna. Since the fields away from the antenna are well behaved, a coarser mesh spacing can be used to substantially reduce

the required computational overhead, as in [12]. A coarse mesh using cells of size $N_c\Delta_r \times N_c\Delta_z$ were used, as opposed to $\Delta_r \times \Delta_z$ for the fine mesh cells. A value of $N_c = 3$ was generally chosen. The interface between the fine and coarse meshes is specified by the user through i_{inner} and j_{inner}. The alignment of the meshes is shown in Figure 2.7. Note that the upper edges of the lowest cell in both the fine and coarse grids was aligned with $z = 0$.

To calculate $E_r(i, j_{inner})$ for the fine mesh along the top of the cylindrical interface, $H_\phi(i/N_c, j_{inner}/N_c + 1)$ from the coarse mesh and $H_\phi(i, j_{inner} - (N_c-1)/2)$ from the fine mesh were first used for values of i which were multiples of N_c. The remainder of the fine mesh E_r values were obtained from these values using linear interpolation. A similar procedure was followed for E_z along the side of the cylindrical interface at $i = i_{inner} - (N_c - 1)/2 - 1$ for the fine mesh. The same time steps were used for the fine and coarse meshes. Stability for the coarse mesh follows automatically if it exists for the fine mesh.

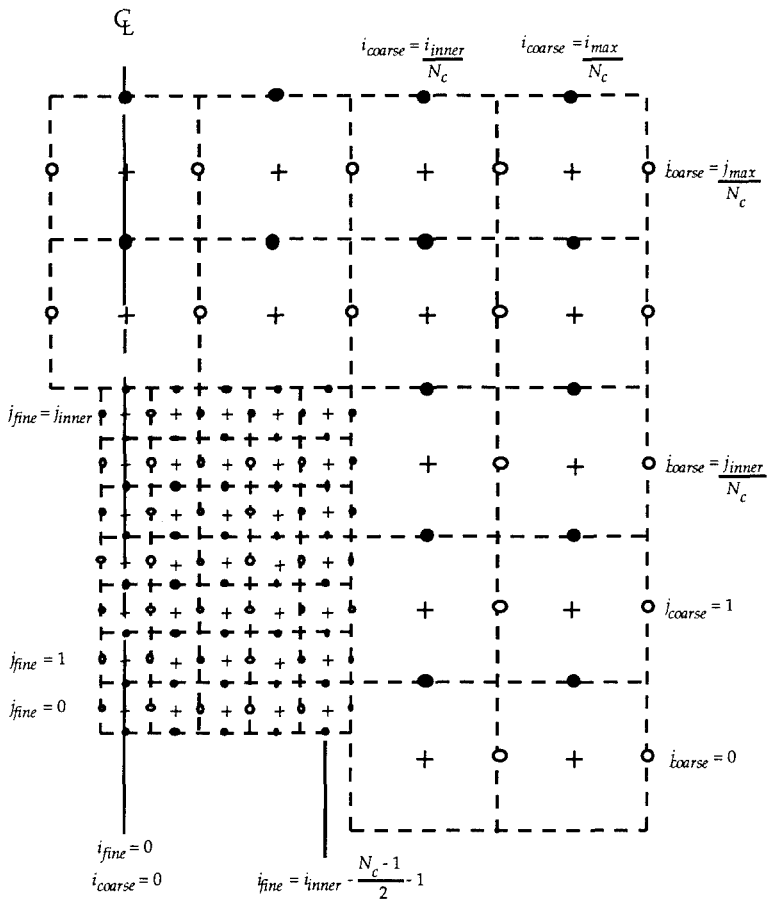

Figure 2.7: Fine/coarse mesh interface detail

2.8 Summary

In this section, the techniques used for the rotationally symmetric FDTD calculation were discussed. While based on the simple Yee algorithm, the contour path technique was used to accommodate arbitrarily shaped boundaries without resorting to the staircase approximation. While this approach was adopted in a limited sense by Maloney and Smith [21], this is the first time to the authors' knowledge that this technique has been applied generally in cylindrical geometry.

A simple absorbing boundary condition was used to terminate the outer limits of the mesh. The electric field in the far field region was calculated by integrating the retarded fields over a cylindrical surface enclosing the antenna. The efficiency of the antenna could be found and conservation of energy verified by integrating the radiated power over the same cylindrical surface used for the far field calculation. To reduce the computational effort required to calculate the fields sufficiently far from the antenna for the absorbing boundary conditions to be valid, a coarse mesh was used to surround the inner fine mesh covering the antenna.

This FDTD calculation was implemented in the program **fdtd_cyl**. In the next section, results obtained from this analysis for spherically capped conical monopoles are compared with results from an analytic treatment. Theoretical predictions for both conical and cylindrical monopoles are compared to experimental data.

3. Conical Monopole D-dot Sensor Analysis

3.1 Introduction

A small conical monopole antenna on a ground plane which is used as a D-dot sensor for transient electromagnetics research was analysed, with parameters a = 0.625 mm, b = 2.1 mm for the coaxial feed, h = 9 mm, h' = 0, and α = 47°. The dielectric constant in the coax was calculated so that the impedance of the feed line was 50 Ω, as required. This meant that only the physical dimensions of the feed line, a, and b, needed to be determined. The angle α corresponds to a 50 Ω characteristic impedance for the monopole. These sensors were initially described by Parkes and Smith [22].

The geometry used for the conical monopole is shown in Figure 3.1. An optional hemispherical cap can be added to the top surface of the cone. The cap was modelled using the simple staircasing technique. This was found to be sufficiently accurate since the cap was sufficiently far from the feed region. The contour path technique was used to model the feed and the conical section of the antenna. Mesh cell dimensions were $\Delta_r = \Delta_z$ = 0.31 mm for the fine mesh, with i_{inner} = 200, j_{inner} = 300, and $i_{max} = j_{max}$ = 600. The number of fine mesh cells per coarse mesh cell, N_c, was set to 3.

Initially, a Gaussian excitation voltage was used as follows

$$V_{inc}(t) = \exp\left[\frac{-t^2}{2\tau_p^2}\right]$$

with τ_p related to the FWHM pulse width though $t_w = 2.355\ \tau_p$.

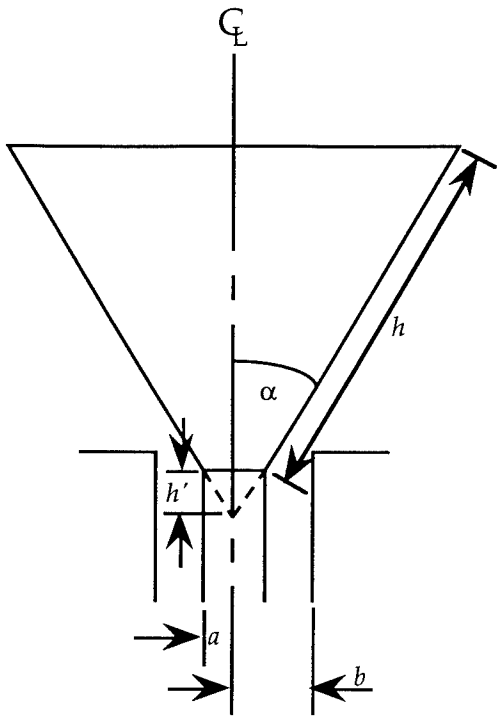

Figure 3.1: Conical monopole geometry

In Appendix A.1, the derivation of a frequency domain mode matching treatment [25-27] is presented. This previously developed technique was used to provide independent verification of the FDTD method. In addition, the calibration of the conical D-dot sensor relies upon various simplifying assumptions discussed in detail in Appendix A.1. These assumptions are used to derive simple results from the full analytic theory which relate the incident electric field to the measured output voltage on the sensor provided the sensor is small compared to the smallest significant wavelength of the incident field.

3.2 Reflected Voltage

From Equation A.17 in Appendix A.1, the input impedance of an ideal electrically small conical monopole can be approximated by a capacitance C_A, where

$$C_A = \frac{h(4\pi Z_c + 3\,\zeta_0 \cos^2\theta_0)}{4\pi c^2 Z_c^2}$$

with ζ_0 the impedance of free space, and Z_c the characteristic impedance of the monopole.

The frequency domain input impedance for the monpole, $Z_A(f)$, was calculated from both the full analytic treatment and the capacitance of an ideal monopole. The time domain reflected voltage, $V_{refl}(t)$, from the antenna back down the feed line was found for a given incident voltage $V_{inc}(t)$ using

$$V_{refl}(t) = \int_{-\infty}^{+\infty} V_{inc}(f)\,\frac{Z_{coax} - Z_A(f)}{Z_{coax} + Z_A(f)}\,\exp(j2\pi ft)\,df$$

where

$$V_{inc}(f) = \int_{-\infty}^{+\infty} V_{inc}\,(t)\,\exp(-j2\pi ft)\,dt$$

The reflected voltage from the full and ideal analytic calculations are compared with the prediction from the FDTD method in Figures 3.2, 3.3, and 3.4 for values of τ_p = 250, 100, and 50 ps, respectively. For all three values of τ_p, the agreement between the FDTD and full analytic results is excellent. This in turn implies that the mode matching calculation correctly models the input impedance of the small conical monopole.

The agreement between the ideal results and the other two methods becomes progressively worse as the pulse width decreases, as expected, since the antenna impedance diverges from a simple capacitance. Since these D-dot sensors are required to work with pulse widths as low as 100 ps (τ_p = 42.46 ps), this discrepancy in the ideal reflected voltage cannot be disregarded when calculating the response of the sensor.

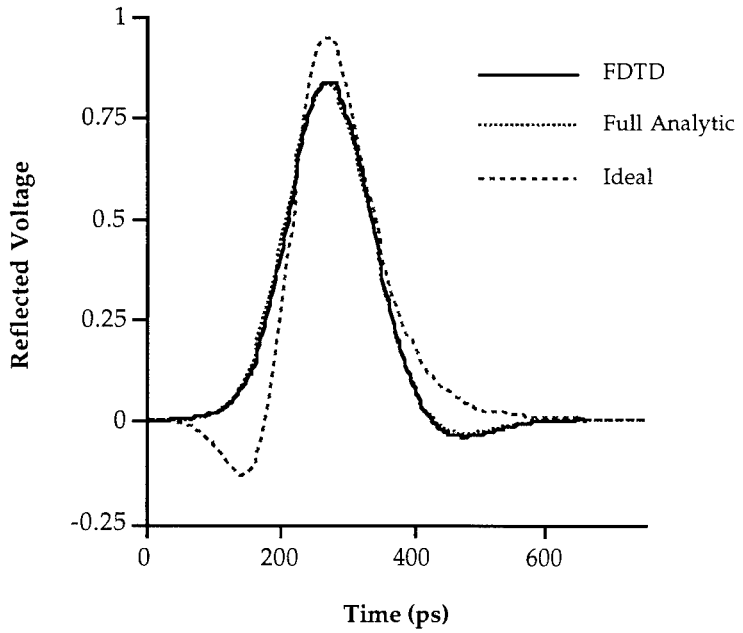

Figure 3.2: Reflected voltage from ideal, full analytic, and FDTD calculations for τ_p *= 50 ps*

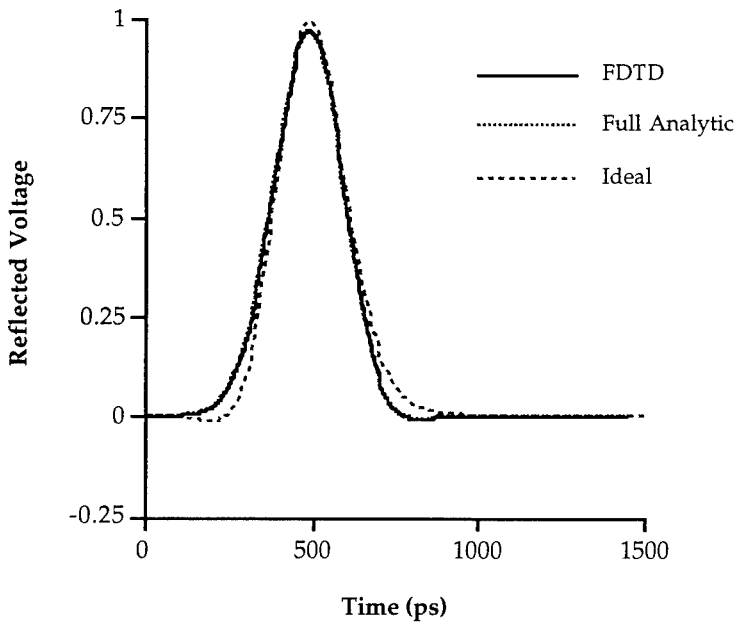

Figure 3.3: Reflected voltage from ideal, full analytic, and FDTD calculations for τ_p *= 100 ps*

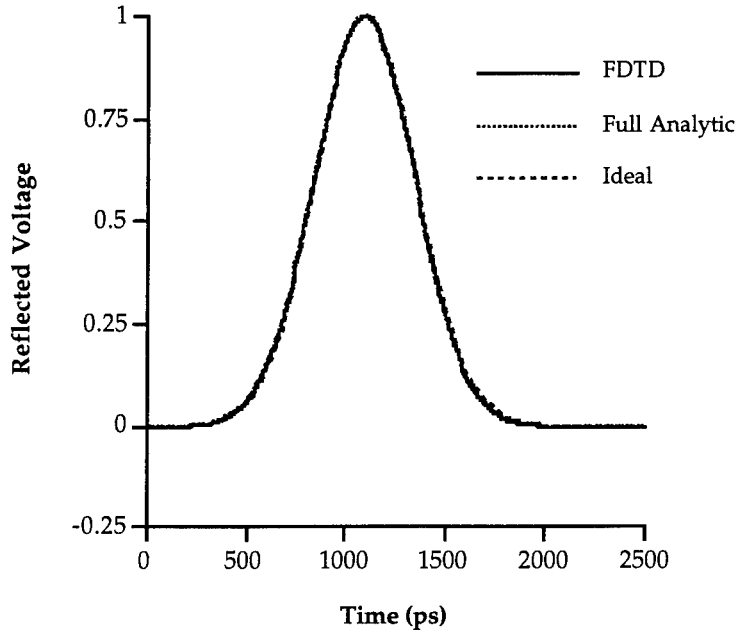

Figure 3.4: Reflected voltage from ideal, full analytic, and FDTD calculations for τ_p = 250 ps

3.3 Transmit Response

In the frequency domain, the transmission transfer function of an antenna is given by

$$T(f) = \frac{E_{rad}(f)}{V_g(f)}$$

$$= j\frac{\zeta_0 f}{cr}\frac{h_e(f)}{Z_A(f) + Z_g}$$

where $V_g(f)$ is the open circuit source voltage, $E_{rad}(f)$ is the radiated far field, $Z_A(f)$ is the antenna impedance, Z_g is the 50 Ω source impedance, and $h_e(f)$ is the effective height of the antenna. The open circuit voltage V_g is twice the input voltage on the coaxial line feeding the antenna if the source, feed line, and antenna characteristic impedance are matched. The parameters $Z_A(f)$, and $h_e(f)$ could be calculated for the conical monopole using Equations A.14, A.15, and A.18 from Appendix A.1. Simple approximations are available for $Z_A(f)$, and $h_e(f)$ in the ideal case of an electrically small monopole.

As discussed in A.6, the time domain radiated electric field $E_{rad}(t)$ on the ground plane ($\theta = 90^o$) in the far field region can be calculated for the full analytic and ideal cases. These results were compared to the predictions from the FDTD analysis for

τ_p = 50, 100, and 250 ps in Figures 3.5, 3.6, and 3.7, respectively. The excitation voltage was a 1 V Gaussian pulse. The $1/R$ dependence has been suppressed, where R is the distance to the far field point. To first order, the simple ideal time domain field for each τ_p calculated using the further assumption discussed in Section A.6 that the monopole impedance $Z_A >> Z_{coax}$. This approximation leads to the simple expression

$$E_{rad}(t) = \frac{3\zeta_0 h^2 \cos\theta_0}{4\pi Z_c r c^2} \frac{d^2 V_g(t)}{dt^2}$$

for the first order time domain radiated field.

From Figures 3.5-3.7, it is clear that good agreement exists between the predictions for the far field derived from the FDTD and analytic techniques. The variation of the electric field E_θ in the far field region predicted by both methods is

$$E_\theta(\theta) = E_\theta(0) \sin\theta$$

as expected for a small monopole. The ideal analytic calculation using small monopole approximations for the antenna impedance and effective height works satisfactorily, but begins to break down at shorter pulse widths as the small monopole approximations break down.

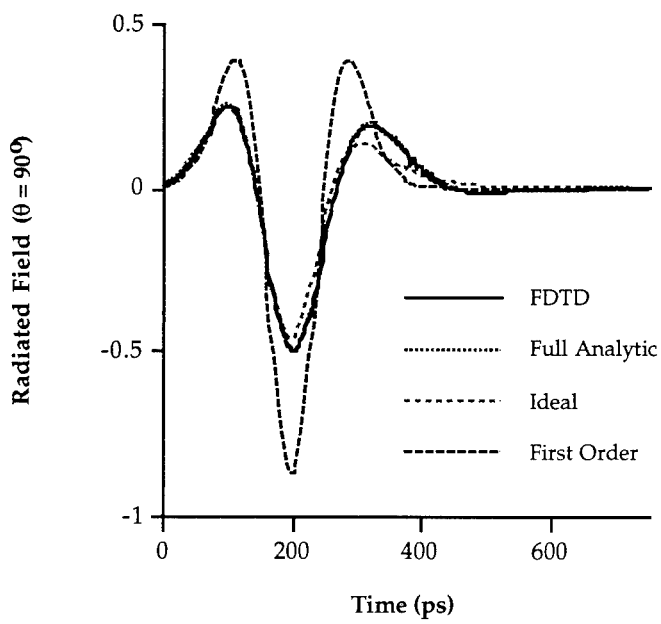

Figure 3.5: FDTD, full and ideal analytic, and first order far field comparison for τ_p = 50 ps

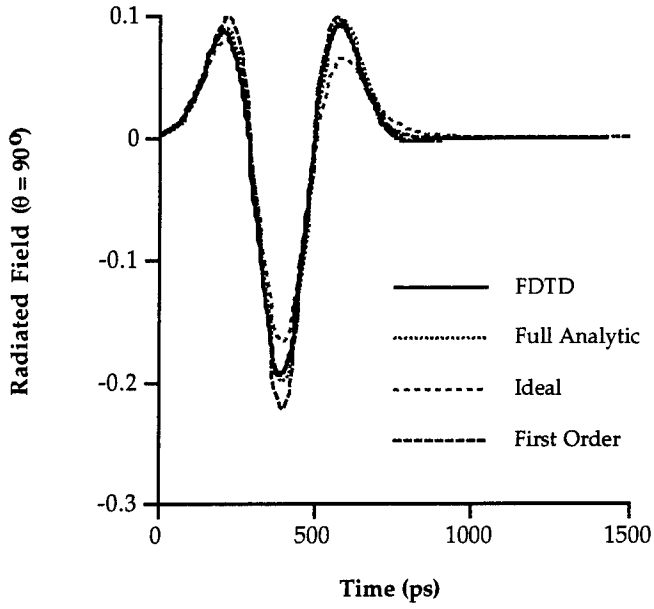

Figure 3.6: FDTD, full and ideal analytic, and first order far field comparison for τ_p = 100 ps

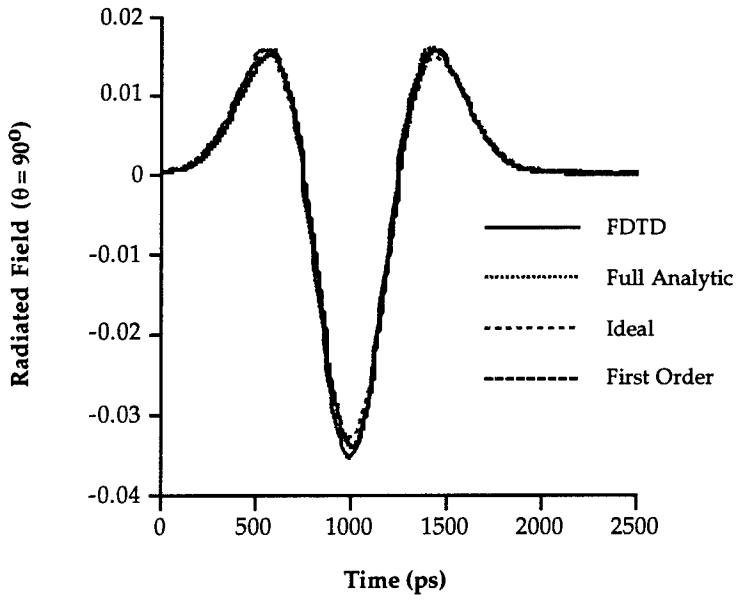

Figure 3.7: FDTD, full and ideal analytic, and first order far field comparison for τ_p = 250 ps

3.4 Receive Response

The receive voltage on the D-dot sensor can be calculated from the transmit response using reciprocity, since the frequency domain receive transfer function S(*f*) for an antenna can be expressed as

$$\begin{aligned} S(f) &= \frac{V_L(f)}{E_{inc}(f)} \\ &= \frac{h_e(f)}{Z_A(f) + Z_L} \end{aligned}$$

where V_L is the receive voltage on the antenna, Z_A is the antenna impedance, and Z_L is the 50 Ω load impedance. For $Z_L = Z_g$ from section 3.3, T(*f*) and S(*f*) are related by

$$S(f) = j\frac{\zeta_0 f}{cr} T(f)$$

Therefore, the probe voltage V_L for an incident field E_{inc} can be calculated for a receive antenna by considering the same antenna in a transmit mode. The radiated field E_{rad} can be calculated from a source voltage V_g which is related to E_{inc} for the receive antenna by

$$V_g(t) = \frac{\zeta_0}{2\pi cr}\frac{dE_{inc}}{dt}$$

Under these circumstances, the receive voltage V_L will be equal to the calculated E_{rad} for the transmit antenna.

For receive monopoles which are small compared to the smallest significant wavelength in the incident field, the voltage developed across the output of the antenna, V_L is related to the incident field E_{inc} to first order by

$$V_L = -\frac{3h^2\cos\theta_0}{2c}\frac{dE_{inc}(t)}{dt}$$

if the angle of arrival of the incident field is 90°, ie. parallel to the ground plane. This equation and the underlying assumptions required to derive it are described in detail in Appendix A.1. For a 9 mm conical monopole, the constant factor is 0.2764 ps/m, as in [22].

Because of the reciprocity relationship, the behaviour of the receive responses follows that of the transmit responses, as shown in Figures 3.8, 3.9, and 3.10 for the specified values of τ_p. The incident field is a vertically polarised Gaussian pulse with a peak amplitude of 1 V/m.

As for the transmit response, the agreement between the full analytic and FDTD predictions is very good. The ideal analytic calculation using small monopole approximations for the antenna impedance and effective height becomes somewhat inaccurate for shorter pulses, as the small monopole approximations breakdown. For τ_p = 50 ps, the first order result shows the worst agreement with the alternative techniques. The breakdown of the first order response relates to the fact that the approximation $Z_A >> Z_{coax}$ is no longer true for the higher frequency components of the shorter incident pulse. Since the approximation $Z_A >> Z_{coax}$ is fundamental in determining the simple D-dot sensor calibration factor used in [22], this can lead to a significant calibration error for shorter pulses. Note that the apparently good agreement between the FDTD and first order analytic techniques at τ_p = 100 ps is merely fortuitous, since the first order response is obtained from the ideal analytic response with further approximation.

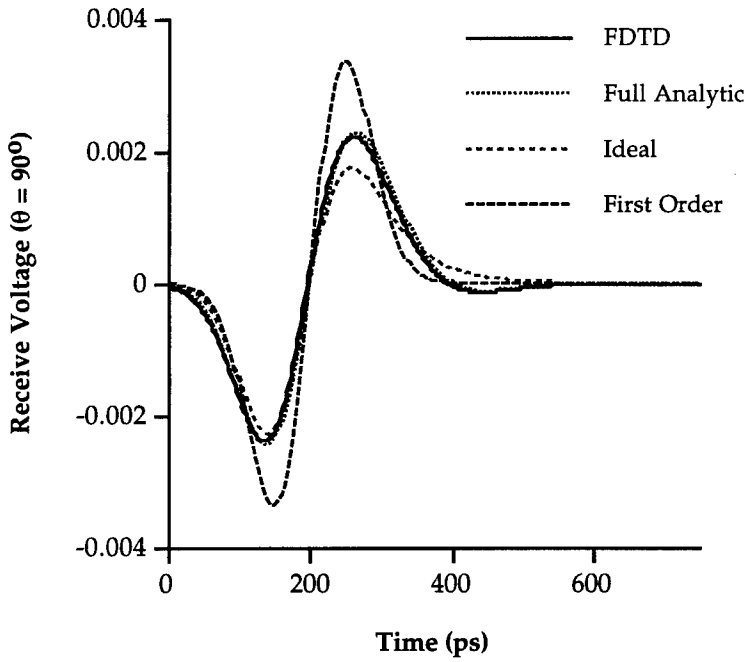

Figure 3.8: FDTD, full and ideal analytic, and first order receive voltage for τ_p = 50 ps

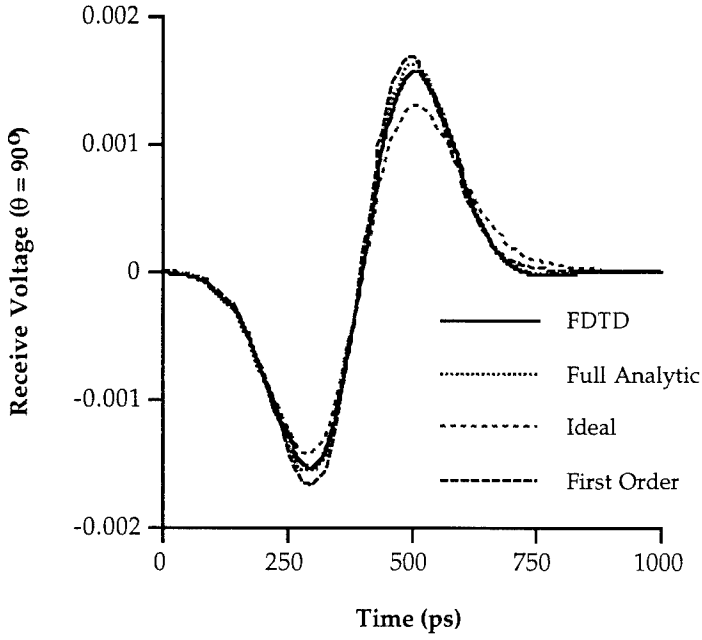

Figure 3.9: FDTD, full and ideal analytic, and first order receive voltage for τ_p = 100 ps

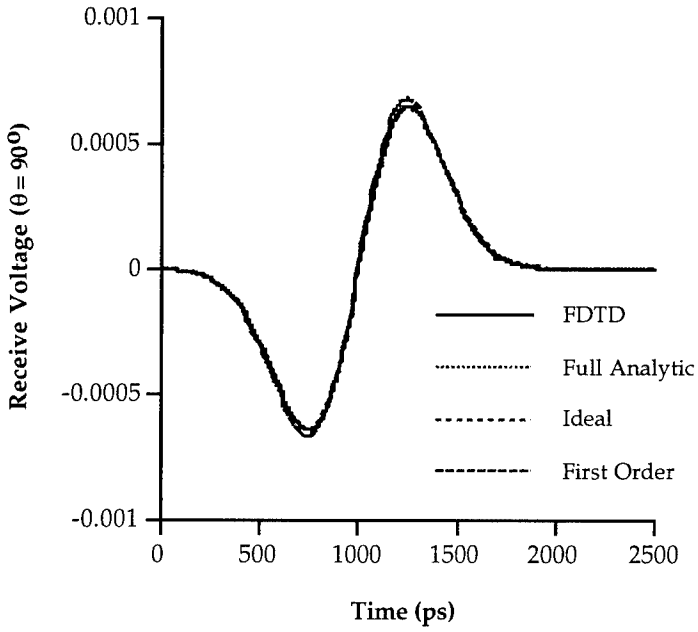

Figure 3.10: FDTD, full and ideal analytic, and first order receive voltage for τ_p = 250 ps

3.5 Comparison of FDTD D-dot Response with Experiment

An experiment was performed to verify the accuracy of the FDTD predictions for the 9mm conical monopole D-dot sensor receive response. A D-dot sensor was mounted on a ground plane 31 cm from a cylindrical monopole with a radius of 6.25 mm and a length of 40 cm. The field at the D-dot site was calculated using the FDTD technique. This field was then used to calculate the output voltage from the 9 mm conical D-dot sensor. The predicted D-dot response was therefore dependent on the accurate FDTD modelling of both the cylindrical monopole and the conical sensor.

A Kentech HMP 1 pulse generator was used to drive the cylindrical monopole with a 3.5 kV, 2 ns pulse with a 100 ps risetime. A Barth 142-NMFP-26 attenuator was used to reduce the Kentech output pulse by 26 dB. The D-dot sensor output voltage and the Kentech output pulse were measured using a Tektronix TDS 820 6 GHz sampling oscilloscope. Data acquisition was performed using a 486 PC with a GPIB interface and LabWindows CVI software.

The measured and predicted conical D-dot sensor output voltages are shown in Figure 3.11. Note that some high frequency components of the applied voltage pulse have been attenuated in the measured data. Note that the FDTD calculation did not include lossy dielectrics or conductors. The agreement between the FDTD results and the measured data is satisfactory, especially since two antennas have been modelled in the process of this comparison.

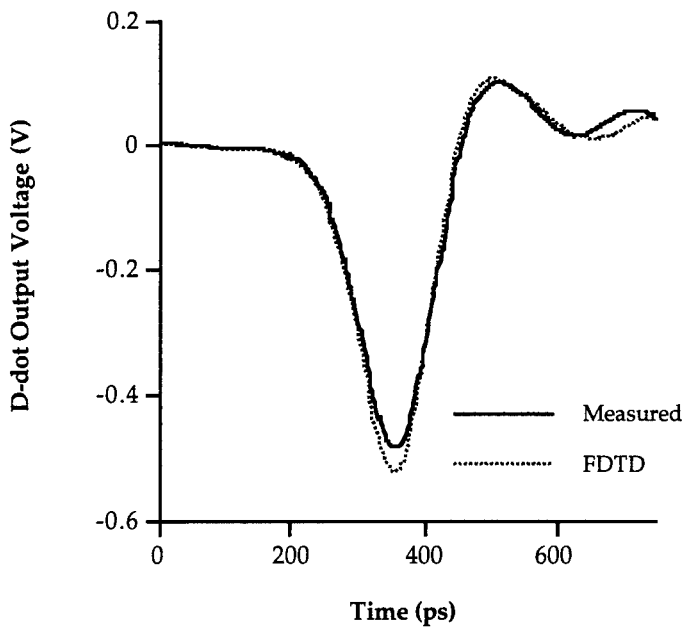

Figure 3.11: Measured and predicted conical D-dot sensor output voltage

The electric field from the cylindrical monopole as calculated by the FDTD technique is shown with the reconstructed electric field from the conical D-dot output voltage. The first order analytic expression in Appendix A.6 derived from the mode matching analysis is used

$$E_{inc}(t) = \frac{2c}{3\zeta_0 a^2 \cos\theta} \int_0^t V_L(t')\, dt'$$

$$= 3.620 \times 10^{-12} \int_0^t V_L(t')\, dt'$$

In Figure 3.12, note that the reconstructed electric field underestimated the calculated field. This is consistent with the discrepancy in Figure 3.11. In addition, Figure 3.8 suggests that for faster pulses, the first order analytic approximation will lead to an underestimate of the measured field. Nevertheless, the agreement is considered sufficiently good for practical purposes.

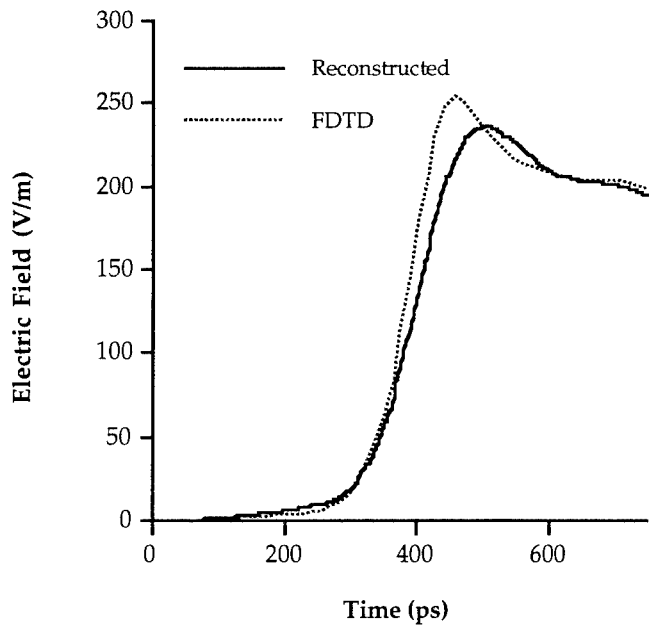

Figure 3.12: Reconstructed and predicted incident field

4. Conclusions

A finite difference time domain (FDTD) technique has been developed to analyse rotationally symmetric antennas such as biconical antennas of arbitrary cross section. The standard Yee formalism was implemented, with a cell deformation technique used to accurately model the feed region. This was necessary to accurately predict the high frequency response of the antenna. A coarse grid surrounding an inner fine grid was used to reduce computational effort for outer regions away from the antenna. Although the FDTD technique calculates only the antenna transmit response directly, the receive response is readily calculated using reciprocity.

A 9 mm conical monopole D-dot sensor on an infinite ground plane was analysed using both the FDTD technique and an analytic technique based on mode matching. The agreement between the two methods was excellent, with the predicted 9 mm conical D-dot sensor response verified by experimental results. The accuracy of approximate techniques based on the analytic mode matching approach was investigated, with some discrepancies with the FDTD technique noted for shorter pulses. Now that its accuracy has been verified by the FDTD method, the full mode matching analysis will be used to more accurately reconstruct incident electric fields from 9 mm conical D-dot measurements for shorter pulses.

Future work will be directed toward interfacing the routine **fdtd_cyl** to CAD software for more convenient design and analysis of rotationally symmetric antennas with arbitrary cross section.

THIS PAGE INTENTIONALLY BLANK

Appendix A

Spherically Capped Conical Monopole Analysis

The frequency domain response of a spherically capped conical monopole antenna on an infinite ground plane as shown in Figure A.1 can be calculated analytically. The response of a biconical antenna with the same dimensions can be determined trivially from the monopole analysis. The fields within the spherical boundary of the antenna are matched to the fields outside the antenna, which is expressed in terms of spherical eigenmodes. This allows the reflection coefficient for the dominant TEM mode at the aperture to be calculated, which in turn yields the antenna driving point impedance and the far field radiation pattern. Because of the requirement for a spherical boundary for field matching, this analysis is restricted to conical monopole antennas with spherical caps. An assumption is made that there is no reflection from the transition between the coax and the antenna feed point.

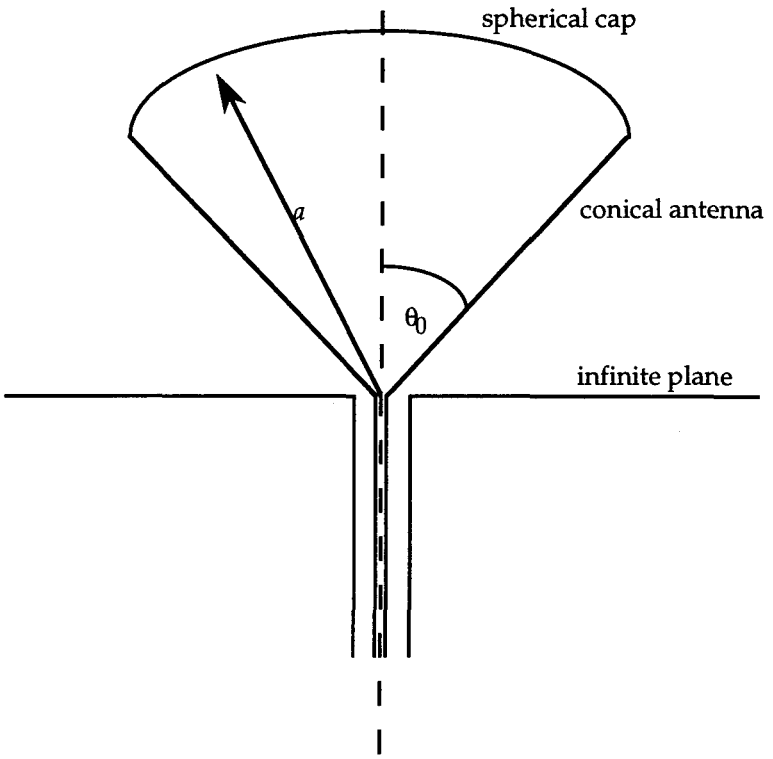

Figure A.1: Conical monopole geometry

A.1 Spherical Eigenmodes

The spherical eigenmodes inside and outside the antenna can be determined from the electric Hertzian potential, since only TM modes are excited. The electric and magnetic fields are written in terms of the Hertzian potential Π_e as

$$\mathbf{H} = j\omega\varepsilon\, \nabla \times \Pi_e \qquad \text{and} \qquad \mathbf{E} = \omega^2\mu_0\varepsilon\Pi_e + \nabla(\nabla.\Pi_e)$$

Since $H_r = 0$ for TM modes, Π_e has only a radial component, so that

$$\Pi_e = \Pi_r\, \mathbf{u}_r = (r\psi)\mathbf{u}_r$$

where ψ is a solution of the scalar Helmholtz equation

$$\nabla^2\psi + k^2\psi(r,\theta) = 0 \qquad \text{where } k^2 = \omega^2\mu_0\varepsilon \text{ [23].}$$

Therefore

$$\frac{1}{r^2}\frac{\partial}{\partial r}\left(r^2\frac{\partial\psi}{\partial r}\right) + \frac{1}{r^2\sin\theta}\frac{\partial}{\partial\theta}\left(\sin\theta\frac{\partial\psi}{\partial\theta}\right) + k^2\psi(r,\theta) = 0$$

This equation is separable, so using $\psi(r,\theta) = R(r)\,\vartheta(\theta)$ results in two equations

$$r^2\frac{d^2R}{dr^2} + 2r\frac{dR}{dr} + (k^2r^2 - p^2)\,R(r) = 0 \tag{A.1}$$

$$\frac{d^2\vartheta}{d\theta^2} + \frac{\cos\theta}{\sin\theta}\frac{d\vartheta}{d\theta} + p^2\vartheta(\theta) = 0 \tag{A.2}$$

where p is the constant of separation. Substituting for $x = \cos\theta$ in (2) yields

$$(1-x^2)\frac{d^2\vartheta}{dx^2} - 2x\frac{d\vartheta}{dx} + \nu(\nu+1)\,\vartheta(x) = 0 \tag{A.3}$$

where $\nu(\nu+1) = p^2$.

The solutions to Equation A.3 are the Legendre functions of the first and second kinds, $P_\nu(\cos\theta)$ and $Q_\nu(\cos\theta)$. These functions are [24]

$$P_\nu(x) = \sqrt{\pi}\left[\frac{F(-\nu, \nu+1; 1; x^2)}{\Gamma(\frac{1}{2}-\frac{\nu}{2})\Gamma(1+\frac{\nu}{2})} - 2x\frac{F(\frac{1}{2}-\frac{\nu}{2}, 1+\frac{\nu}{2}; \frac{3}{2}; x^2)}{\Gamma(\frac{1}{2}+\frac{\nu}{2})\Gamma(-\frac{\nu}{2})}\right]$$

$$Q_\nu(x) =$$

$$\sqrt{\pi}\left[\frac{\Gamma(\frac{1}{2}+\frac{\nu}{2})\cos(\frac{(\nu+1)\pi}{2})\,F(-\frac{\nu}{2},\frac{1}{2}+\frac{\nu}{2},\frac{1}{2};x^2)}{2\,\Gamma(1+\frac{\nu}{2})} + x\,\frac{\Gamma(1+\frac{\nu}{2})\cos(\frac{\nu\pi}{2})\,F(\frac{1}{2}-\frac{\nu}{2},1+\frac{\nu}{2},\frac{3}{2};x^2)}{\Gamma(\frac{1}{2}+\frac{\nu}{2})}\right]$$

where the hypergeometric function is

$$F(a,b;c;x) = \frac{\Gamma(c)}{\Gamma(a)\Gamma(b)}\sum_{n=0}^{\infty}\frac{\Gamma(a+n)\Gamma(b+n)}{\Gamma(c+n)}\frac{x^n}{n!}$$

The solutions to Equation A.1 are the spherical Bessel functions $j_\nu(kr)$ and $y_\nu(kr)$, where

$$j_\nu(z) = \sqrt{\frac{\pi}{2z}}\,J_{\nu+1/2}(z)$$

$$y_\nu(z) = \sqrt{\frac{\pi}{2z}}\,Y_{\nu+1/2}(z)$$

$j_\nu(z)$ and $y_\nu(z)$ can be combined into spherical Hankel functions of the first and second kind to represent waves travelling inward and outward, respectively, relative to the origin.

$$h_\nu^{(1)}(z) = j_\nu(z) + j\,y_\nu(z) \qquad \text{inward travelling wave}$$

$$h_\nu^{(2)}(z) = j_\nu(z) - j\,y_\nu(z) \qquad \text{outward travelling wave}$$

Since the field outside the spherical boundary of the conical monopole must be finite at $\theta = 0$ and π, ν can only take integer values, n. The external field can also only consist of outgoing spherical waves, the scalar function ψ_{out} is given by

$$\psi_{out} = \sum_{n=0}^{\infty}\frac{1}{j\omega\varepsilon}A_n\,h_n^{(2)}(kr)\,P_n(\cos\theta)$$

So

$$\Pi_r = \sum_{n=0}^{\infty} \frac{1}{j\omega\varepsilon} r A_n h_n^{(2)}(kr) P_n(\cos\theta)$$

where A_n are arbitrary and the $1/j\omega\varepsilon$ factor has been included for the sake of consistency with the derivation in [25].

Since $\frac{\partial}{\partial\phi} = 0$, and the TM mode magnetic field has only a ϕ component

$$\mathbf{H} = H_\phi \mathbf{u}_\phi = -j\omega\varepsilon \frac{1}{r}\frac{\partial \Pi_r}{\partial\theta}\mathbf{u}_\phi$$

$$= -\sum_{n=0}^{\infty} A_n h_n^{(2)}(kr) \frac{d}{d\theta} P_n(\cos\theta)$$

$$= \sum_{n=0}^{\infty} A_n h_n^{(2)}(kr) \sin\theta\, P_n'(\cos\theta)$$

The electric field outside the conical monopole is readily determined from the magnetic field using

$$\mathbf{E} = \frac{1}{j\omega\varepsilon} \nabla \times \mathrm{H}$$

Consider

$$E_r = \frac{1}{jkr\sin\theta}\sqrt{\frac{\mu_0}{\varepsilon}}\frac{\partial}{\partial\theta}(H_\phi \sin\theta)$$

Since

$$\frac{d}{d\theta}\left(\sin\theta \frac{dP_n(\cos\theta)}{d\theta}\right)$$

$$= \sin\theta \frac{d^2P_n(\cos\theta)}{d\theta^2} + \cos\theta \frac{dP_n(\cos\theta)}{d\theta}$$

$$= -\sin\theta\cos\theta\, P_n'(\cos\theta) + \sin^3\theta\, P_n''(\cos\theta) - \sin\theta\cos\theta\, P_n'(\cos\theta)$$

$$= -2\sin\theta\cos\theta\, P_n'(\cos\theta) + \sin^3\theta\, P_n''(\cos\theta)$$

E_r can be calculated from

$$E_r = -j\sqrt{\frac{\mu_0}{\varepsilon}}\frac{1}{kr\sin\theta}$$

$$\sum_{n=0}^{\infty} A_n\, h_n^{(2)}(kr)\,(2\sin\theta\cos\theta\, P_n'(\cos\theta) - \sin^3\theta\, P_n''(\cos\theta))$$

$$= -j\sqrt{\frac{\mu_0}{\varepsilon}}\sum_{n=0}^{\infty} A_n \frac{h_n^{(2)}(kr)}{kr}\, n(n+1)\sin\theta\, P_n(\cos\theta)$$

since

$$(1-x^2)\, P_n''(x) - 2xP_n'(x) + n(n+1)\, P_n(x) = 0$$

Similarly E_θ can be determined from

$$E_\theta = -\frac{1}{jkr}\sqrt{\frac{\mu_0}{\varepsilon}}\frac{d}{dr}(rH_\phi)$$

with

$$\frac{d}{dr}(rh_n^{(2)}(kr)) = h_n^{(2)}(kr) + kr\, h_n^{(2)'}(kr)$$

$$= kr\, h_{n-1}^{(2)}(kr) - n\, h_n^{(2)}(kr)$$

Therefore

$$E_\theta = j\sqrt{\frac{\mu_0}{\varepsilon}}\sum_{n=0}^{\infty}\frac{A_n}{kr}\sin\theta\, P_n'(\cos\theta)\,(kr\, h_{n-1}^{(2)}(kr) - n\, h_n^{(2)}(kr))$$

$$= j\sqrt{\frac{\mu_0}{\varepsilon}}\sum_{n=0}^{\infty} A_n\sin\theta\, P_n'(\cos\theta)\,(h_{n-1}^{(2)}(kr) - \frac{n}{kr}h_n^{(2)}(kr))$$

Since the field inside the spherical boundary of the conical monopole is not required to be finite at $\theta = 0$ and π, and consists of both ingoing and outgoing spherical waves, the scalar function ψ_{in} is given by

$$\psi_{in} = \sum_{\nu=0}^{\infty} \frac{1}{j\omega\varepsilon} (A_\nu h_\nu^{(2)}(kr) + B_\nu h_\nu^{(1)}(kr)) (P_\nu(\cos\theta) + \alpha_\nu Q_\nu(\cos\theta))$$

Although the mode spectrum is discrete, note that ν is not restricted to integer values. The coefficients A_ν refer to modes propagating outward from the origin, while the B_ν coefficients relate to modes reflected from the aperture and travelling inward towards the origin. Using the scalar function ψ_{in} and proceeding as for the fields outside the spherical boundary of the conical monopole yields the fields inside the interface as follows

$$H_\phi = -\sum_{\nu=0}^{\infty} (A_\nu h_\nu^{(2)}(kr) + B_\nu h_\nu^{(1)}(kr)) \left(\frac{d}{d\theta}P_\nu(\cos\theta) + \alpha_\nu \frac{d}{d\theta}Q_\nu(\cos\theta)\right)$$

$$E_r = -j\sqrt{\frac{\mu_0}{\varepsilon}} \sum_{\nu=0}^{\infty} \left(A_\nu \frac{h_\nu^{(2)}(kr)}{kr} + B_\nu \frac{h_\nu^{(1)}(kr)}{kr}\right) \nu(\nu+1) \sin\theta \, (P_\nu(\cos\theta) + \alpha_\nu Q_\nu(\cos\theta))$$

$$E_\theta = -j\sqrt{\frac{\mu_0}{\varepsilon}} \sum_{\nu=0}^{\infty} \left(A_\nu\left(h_{\nu-1}^{(2)}(kr) - \frac{\nu}{kr} h_\nu^{(2)}(kr)\right) + B_\nu\left(h_{\nu-1}^{(1)}(kr) - \frac{\nu}{kr} h_\nu^{(1)}(kr)\right)\right) \left(\frac{d}{d\theta}P_\nu(\cos\theta) + \alpha_\nu \frac{d}{d\theta}Q_\nu(\cos\theta)\right)$$

Values of ν corresponding to TM mode solutions are determined from the boundary condition on the side of the conical conductors, $E_r = 0$ at $\theta = \theta_0$ and $\theta = \pi - \theta_0$. Therefore

$$\nu(\nu+1) \sin\theta \, (P_\nu(\cos\theta_0) + \alpha_\nu Q_\nu(\cos\theta_0)) = 0 \qquad \text{(A.4)}$$

and

$$\nu(\nu+1)\ (P_\nu(-\cos\theta_0) + \alpha_\nu Q_\nu(-\cos\theta_0)) \quad = \ 0 \qquad (A.5)$$

with symmetry requiring

$$\nu(\nu+1)\ (P_\nu(0) + \alpha_\nu Q_\nu(0)) \quad = \ 0 \qquad (A.6)$$

These conditions are trivially satisfied for the lowest order TM mode, the TEM mode ($\nu = 0$). There is no contribution to the fields from the $P_0(\cos\theta)$ term since $\frac{dP_0}{d\theta} = 0$. Therefore the TEM fields inside the conical monopole are

$$H_\phi^{TEM} = -(A_0\, h_0^{(2)}(kr) + B_0\, h_0^{(1)}(kr))\, \frac{d}{d\theta} Q_0(\cos\theta)$$

$$= \frac{j}{kr\sin\theta} A_0\ (\exp(-jkr) - \rho\ \exp(jkr)) \qquad (A.7)$$

$$E_\theta^{TEM} = -j\sqrt{\frac{\mu_0}{\varepsilon}}\,(A_0 h_{-1}^{(2)}(kr) + B_0 h_{-1}^{(1)}(kr))\, \frac{d}{d\theta} Q_0(\cos\theta)$$

$$= -j\sqrt{\frac{\mu_0}{\varepsilon}}\ A_0\ \frac{\exp(-jkr) + \rho\ \exp(jkr)}{kr\sin\theta} \qquad (A.8)$$

where the α_0 factor has been absorbed into A_0 and B_0, $\rho = B_0/A_0$ is the reflection coefficient, and the following expressions have been used

$$Q_0(\cos\theta) = \frac{1}{2}\ln\left[\frac{1+\cos\theta}{1-\cos\theta}\right]$$

$$\frac{d}{d\theta} Q_0(\cos\theta) = \frac{1}{\sin\theta}$$

$$h_0^{(1)}(kr) = -j\, h_{-1}^{(1)}(kr) = -\frac{j}{kr}\exp(jkr)$$

$$h_0^{(2)}(kr) = j\, h_{-1}^{(2)}(kr) = \frac{j}{kr}\exp(-jkr)$$

The evaluation of higher order TM modes will require the calculation of the mode number n. This is performed by solving the boundary condition Equations A.4, A.5, and A.6.

A.2 Aperture Field Matching

In practical conical monopole antennas, all modes inside the antenna except for the TEM mode are cutoff. Since this mode cannot exist outside the antenna, power is radiated by higher order TM modes which are excited by the TEM wave at the aperture. The scattering coefficients which determine the amplitudes of the TM eigenmodes outside the antenna can be determined by matching the transverse component of the electric field, E_θ at the aperture ($r = a$). Inside the antenna the approximation made by Pappas and King [25, 26] is used which ignores the contribution from all higher order evanescent modes inside the spherical interface. This approximation will be a fundamental limit to the accuracy of this technique unless higher order modes are included. The electric field inside the antenna is therefore given by

$$E_\theta = -j A_0 \sqrt{\frac{\mu_0}{\varepsilon}} \frac{\exp(-jka) + \rho \exp(jka)}{ka \sin\theta} \qquad \text{over the aperture } (\theta_0 < \theta < \pi-\theta_0)$$

$$= 0 \qquad \text{over spherical cap}$$

where ρ is the reflection coefficient which accounts for TEM mode reflection at the aperture discontinuity. The field outside the antenna is

$$E_\theta = -j \sqrt{\frac{\mu_0}{\varepsilon}} \sum_{n=0}^{\infty} A_n \left(h_{m-1}^{(2)}(ka) - \frac{m}{ka} h_m^{(2)}(ka)\right) \frac{d}{d\theta} P_m(\cos\theta)$$

Equating the fields inside and outside the aperture leads to

$$\frac{A_0}{ka \sin\theta} (\exp(-jka) + \rho \exp(jka)) = \sum_{m=0}^{\infty} A_m \left(h_{m-1}^{(2)}(ka) - \frac{m}{ka} h_m^{(2)}(ka)\right) \frac{d}{d\theta} P_m(\cos\theta)$$

Following the method of Papas and King [25, 26], multiplying both sides by $\sin\theta \frac{d}{d\theta} P_n(\cos\theta)$ and integrating over the spherical interface from $\theta = 0$ to π yields

$$A_0 (\exp(-jka) + \rho \exp(jka)) \int_{\theta_0}^{\pi-\theta_0} \left(\frac{d}{d\theta} P_n(\cos\theta)\right) d\theta = 2 A_0 P_n(\cos\theta_0) (\exp(-jka) + \rho \exp(jka))$$

$$= \sum_{m=0}^{\infty} ka\ A_m(h^{(2)}_{m-1}(ka) - \frac{m}{ka} h^{(2)}_m(ka)) \int_0^{\pi} \sin\theta \frac{d}{d\theta}P_n(\cos\theta)\frac{d}{d\theta} P_m(\cos\theta)\, d\theta$$

$$= 2\, ka\, A_n \frac{n(n+1)}{2n+1} (h^{(2)}_{n-1}(ka) - \frac{n}{ka} h^{(2)}_n(ka))$$

where the following orthogonality relation has been used [27]

$$\int_0^{\pi} \sin\theta \frac{d}{d\theta}P_n(\cos\theta)\frac{d}{d\theta} P_m(\cos\theta)\, d\theta = \frac{2n(n+1)}{2n+1}\delta_{mn}$$

Because of the antenna symmetry, only odd n need be considered. Therefore the spherical eigenmode amplitudes in the region outside the interface are given by

$$A_n = A_0 \frac{\exp(-jka) + \rho \exp(jka)}{ka} \frac{2n+1}{n(n+1)} P_n(\cos\theta_0) \frac{1}{h^{(2)}_{n-1}(ka) - \frac{n}{ka} h^{(2)}_n(ka)} \qquad (A.9)$$

Using the substitution for A_n in Equation A.9, the electric field outside the antenna can be related to the reflection coefficient ρ and the amplitude of the outward travelling TEM mode in the antenna A_0 by

$$E_\theta = -j A_0 \sqrt{\frac{\mu_0}{\varepsilon}} \frac{\exp(-jka) + \rho \exp(jka)}{ka}$$

$$\sum_{n\ odd}^{\infty} \frac{2n+1}{n(n+1)} \frac{h^{(2)}_{n-1}(kr) - \frac{n}{kr} h^{(2)}_n(kr)}{h^{(2)}_{n-1}(ka) - \frac{n}{ka} h^{(2)}_n(ka)} P_n(\cos\theta_0)\frac{d}{d\theta}P_n(\cos\theta) \qquad (A.10)$$

where the summation is over odd n only. In the far field region where $kr \to \infty$, the term

$$h^{(2)}_{n-1}(kr) - \frac{n}{kr} h^{(2)}_n(kr) \to \frac{j^n \exp(-jkr)}{kr}$$

From Equation A.10, the electric field in the far field region is therefore

$$E_\theta = -j A_0 \sqrt{\frac{\mu_0}{\varepsilon}} \frac{\exp(-jkr)}{kr} \frac{\exp(-jka) + \rho \exp(jka)}{ka}$$

$$\sum_{n\ odd}^{\infty} \frac{2n+1}{n(n+1)} \frac{j^n}{h_{n-1}^{(2)}(ka) - \frac{n}{ka} h_n^{(2)}(ka)} P_n(\cos\theta_0) \frac{d}{d\theta} P_n(\cos\theta) \qquad \text{(A.11)}$$

The electric field can be expressed in terms of the current I_0 through the centre conductor at the feed point. Consider a circular patch of radius r_c on the ground plane which encloses the centre conductor of the monopole. Ampere's law states that

$$\oint_C \mathbf{H}.dl = I_0 + \frac{\partial}{\partial t} \iint_S \varepsilon \mathbf{E}.dS$$

For the circular patch

$$\int_0^{2\pi} r_c H_\phi \, d\phi = I_0 + \frac{\partial}{\partial t} \int_0^{r_c} \int_0^{2\pi} \varepsilon \, r \, E_\theta \, d\phi \, dr$$

Because the monopole is azimuthally symmetric

$$2\pi H_\phi r = I_0 + F(\partial,\partial t) \int_0^{r_c} 2\pi\varepsilon \, r \, E_\theta \, dr$$

Substituting for H_ϕ and E_θ from Equation A.7 and A.8 leads to

$$\frac{j2\pi}{k} A_0 \left(\exp(-jkr_c) - \rho \exp(jkr_c)\right) = I_0 + \frac{j2\pi}{k} A_0 \left[\exp(-jkr_c) - \rho \exp(jkr_c) - (1-\rho)\right]$$

At the feed point where $r_c \rightarrow 0$, the second term on the right tends to 0, so that the amplitude of the outward TEM electric field in the monopole is related to the applied current by

$$A_0 = \frac{kI_0}{j2\pi(1-\rho)}$$

By substituting for A_0 in Equation A.11, the electric field in the far field region can be expressed in terms of the feed current I_0 and the TEM mode reflection coefficient ρ as

$$E_\theta = -\sqrt{\frac{\mu_0}{\varepsilon}} \frac{I_0}{2\pi(1-\rho)} \frac{\exp(-jkr)}{r} \frac{\exp(-jka) + \rho \exp(jka)}{ka}$$

$$\sum_{n\ odd}^{\infty} \frac{2n+1}{n(n+1)} \frac{j^n}{h_{n-1}^{(2)}(ka) - \frac{n}{ka} h_n^{(2)}(ka)} P_n(\cos\theta_0) \frac{d}{d\theta} P_n(\cos\theta) \qquad \text{(A.12)}$$

This is identical to Equation 8 in [27]. According to Harrison and Williams [27], the effective height of the conical monopole is defined as

$$kh_e(f) = \frac{E_\theta(f)}{(j\zeta_0/2\pi)\,(\exp(-jkr)/r)\,I_0(f)} \qquad \text{(A.13)}$$

where $\zeta_0 = \sqrt{\mu_0/\varepsilon}$ is the impedance of free space.

Using

$$h_n^{(2)}(kr) \rightarrow \frac{-j^{n-1}\exp(-jkr)}{kr}$$

as $kr \rightarrow \infty$, the magnetic field in the far field region is therefore

$$H_\phi = -\frac{I_0}{2\pi(1-\rho)} \frac{\exp(-jkr)}{r} \frac{\exp(-jka) + \rho\exp(jka)}{ka}$$

$$\sum_{n\ odd}^{\infty} \frac{2n+1}{n(n+1)} \frac{j^n}{h_{n-1}^{(2)}(ka) - \frac{n}{ka} h_n^{(2)}(ka)} P_n(\cos\theta_0) \frac{d}{d\theta} P_n(\cos\theta)$$

$$= \frac{E_\theta}{\zeta_0}$$

Provided the TEM mode reflection coefficient ρ can be determined, the fields outside the antenna can be calculated. To calculate ρ, the tangential component of the magnetic field, H_ϕ, is matched over the aperture

$$\frac{j}{ka\sin\theta}(\exp(-jka) - \rho\exp(jka)) = \sum_{n=0}^{\infty} A_n h_n^{(2)}(ka) \frac{d}{d\theta} P_n(\cos\theta)$$

Multiplying both sides by $\sin\theta \frac{d}{d\theta} Q_0(\cos\theta)$ and integrating over the spherical interface from $\theta = \theta_0$ to $\pi-\theta_0$ leads to

$$\frac{j}{ka}(\exp(-jka) - \rho\exp(jka))\int_{\theta_0}^{\pi-\theta_0}\frac{d\theta}{\sin\theta}\,d\theta = -2\frac{j}{ka}(\exp(-jka) - \rho\exp(jka))\ln\cot\left(\frac{\theta_0}{2}\right)$$

$$= -\frac{\exp(-jka) + \rho\exp(jka)}{ka}\sum_{n=0}^{\infty}\frac{2n+1}{n(n+1)}P_n(\cos\theta_0)\,\zeta_n(ka)\int_{\theta_0}^{\pi-\theta_0}\left(\frac{d}{d\theta}P_n(\cos\theta)\right)d\theta$$

$$= 2\frac{\exp(-jka) + \rho\exp(jka)}{ka}\sum_{n=0}^{\infty}\frac{2n+1}{n(n+1)}[P_n(\cos\theta_0)]^2\,\zeta_n(ka)$$

where

$$\zeta_n(ka) = \frac{h_n^{(2)}(ka)}{h_{n-1}^{(2)}(ka) - \frac{n}{ka}h_n^{(2)}(ka)}$$

Therefore

$$(\exp(-jka) - \rho\exp(jka)) = -(\exp(-jka) + \rho\exp(jka))\frac{j\zeta_0}{2\pi Z_c}\sum_{n=0}^{\infty}\frac{2n+1}{n(n+1)}[P_n(\cos\theta_0)]^2\,\zeta_n(ka)$$

where Z_c is the characteristic TEM mode impedance of an infinitely long conical monopole given by

$$Z_c = \frac{\zeta_0}{2\pi}\ln\cot\left(\frac{\theta_0}{2}\right)$$

Consider

$$\exp(-j2ka) - \rho = -\gamma(\exp(-j2ka) + \rho)$$

so that

$$\rho = \exp(-j\,2ka)\,\frac{1+\gamma}{1-\gamma}$$

$$= \exp(-j\,2ka)\left[\frac{1 + j\frac{\zeta_0}{2\pi Z_c}\sum_{n\ odd}^{N}\frac{(2n+1)}{n(n+1)}\,[P_n(\cos(\theta_0))]^2\,\zeta_n(ka)}{1 - j\frac{\zeta_0}{2\pi Z_c}\sum_{n\ odd}^{N}\frac{(2n+1)}{n(n+1)}\,[P_n(\cos(\theta_0))]^2\,\zeta_n(ka)}\right] \qquad (A.14)$$

where the summation is over $n = 1, 3, 5, \ldots, N$.

Now that the TEM mode reflection coefficient has been determined, the fields outside the conical monopole can be calculated using the modal coefficients A_n. This result has been presented in [25-27]. The impedance of the finite bicone antenna is therefore

$$Z_A(f) = Z_c\,\frac{1+\rho}{1-\rho} \qquad (A.15)$$

A.3 Power Conservation

Conservation of power across the spherical interface separating the regions inside and outside the spherical boundary was used to assess the influence of neglecting higher order modes within the antenna. Inside the antenna, the TEM electric and magnetic fields can be used to calculate the power crossing the interface, P_r, at $r = a$ using

$$P_r^{in} = \pi a^2 \int_{\theta_0}^{\pi/2} \mathrm{Re}\{E_\theta(a,\theta)\,H_\phi(a,\theta)^*\}\,\sin\theta\,d\theta$$

$$= \frac{I_0^2\,\zeta_0}{4\pi(1-\rho)^2}\,(1 - \rho^2 + \mathrm{Re}\{\rho\,\exp(j2ka) - \rho^*\,\exp(-j2ka)\})\int_{\theta_0}^{\pi/2}\frac{1}{\sin\theta}\,d\theta$$

$$= \frac{I_0^2\,\zeta_0}{4\pi(1-\rho)^2}\,(1 - \rho^2 + \mathrm{Re}\{\rho\,\exp(j2ka) - \rho^*\,\exp(-j2ka)\})\,\ln\cot\left(\frac{\theta_0}{2}\right)$$

$$= \frac{I_0^2\,Z_c}{2}\,\frac{1 - \rho^2 + \mathrm{Re}\{\rho\,\exp(j2ka) - \rho^*\,\exp(-j2ka)\}}{(1-\rho)^2}$$

Note that if there is no reflection from the interface, then all of the applied power is radiated. The applied power is given by

$$P_r^{app} = \frac{I_0^2 Z_c}{2}$$

Using Equation A.12, the power crossing a hemispherical boundary surrounding the antenna at $r \to \infty$ is given by

$$P_r^{out} = \pi r^2 \int_{\theta_0}^{\pi/2} \mathrm{Re}\{E_\theta(r,\theta)\, H_\phi(r,\theta)^*\} \sin\theta \, d\theta$$

$$= \frac{I_0^2 \zeta_0}{4\pi(1-\rho)^2} (1 + \rho^2 + \mathrm{Re}\{\rho \exp(j2ka) + \rho^* \exp(-j2ka)\})$$

$$\sum_{m\ odd}^{N} \sum_{n\ odd}^{N} \frac{(2m+1)(2n+1)}{m(m+1)n(n+1)} \frac{-j^{n+m} P_m(\cos(\theta_0))\, P_n(\cos(\theta_0))}{\left[ka\, h_{n-1}^{(2)}(ka) - n\, h_n^{(2)}(ka)\right]\left[ka\, h_{m-1}^{(2)}(ka) - m\, h_m^{(2)}(ka)\right]}$$

$$\int_0^{\pi/2} \sin\theta \frac{d}{d\theta} P_n(\cos\theta) \frac{d}{d\theta} P_m(\cos\theta)\, d\theta$$

Since

$$\int_0^{\pi} \sin\theta \frac{d}{d\theta} P_n(\cos\theta) \frac{d}{d\theta} P_m(\cos\theta)\, d\theta = \frac{2n(n+1)}{2n+1} \delta_{mn}$$

the radiated power in the far field region is given by

$$P_r^{out} = \frac{I_0^2 \zeta_0}{4\pi(1-\rho)^2} (1 + \rho^2 + \mathrm{Re}\{\rho \exp(j2ka) + \rho^* \exp(-j2ka)\})$$

$$\sum_{n\ odd}^{N} \frac{(2n+1)}{n(n+1)} \frac{(-1)^{n+1} [P_n(\cos(\theta_0))]^2}{\left[ka\, h_{n-1}^{(2)}(ka) - n\, h_n^{(2)}(ka)\right]^2}$$

Power conservation across the spherical interface separating the inner and outer regions of the monopole was verified to a high degree of accuracy in the frequency domain up to at least $ka = 100$ using $N = 59$ for the summation terms.

A.4 Small Conical Monopole Approximation

For electrically short monopoles with $ka << 1$, a number of simplifying approximations can be used to calculate the input impedance. Consider the summation term from Equation A.14

$$S = j\frac{\zeta_0}{2\pi Z_c}\sum_{n\ odd}^{N}\frac{(2n+1)}{n(n+1)}[P_n(\cos(\theta_0))]^2\,\zeta_n(ka))$$

For small ka

$$\zeta_n = \frac{h_n^{(2)}(ka)}{h_{n-1}^{(2)}(ka) - \frac{n}{ka}h_n^{(2)}(ka)}$$

$$\approx -\frac{ka}{n}$$

Hence

$$S \approx -j\frac{\zeta_0 ka}{2\pi Z_c}\sum_{n\ odd}^{N}\frac{(2n+1)}{n^2(n+1)}[P_n(\cos(\theta_0))]^2$$

For $\theta_0 = 47^o$ corresponding to a characteristic impedance of 50 Ω, then the dominant term will correspond to $n = 1$. The next highest contribution will be from the $n = 3$ term which is only 1.5 % of the $n = 1$ term. Therefore S can be approximated by

$$S \approx -j\frac{3\zeta_0 ka}{4\pi Z_c}\cos^2(\theta_0)$$

The reflection coefficient ρ is given by

$$\rho = \exp(-j\,2ka)\left[\frac{1 - j\frac{3\zeta_0}{4\pi Z_c}ka\cos^2(\theta_0)}{1 + j\frac{3\zeta_0}{4\pi Z_c}ka\cos^2(\theta_0)}\right]$$

$$\approx \frac{1 - jka}{1 + jka}\left[\frac{1 - j\frac{3\zeta_0}{4\pi Z_c} ka \cos^2(\theta_0)}{1 + j\frac{3\zeta_0}{4\pi Z_c} ka \cos^2(\theta_0)}\right]$$

$$\approx \frac{1 - j\frac{ka}{4\pi Z_c}(3\zeta_0 \cos^2(\theta_0) + 4\pi Z_c)}{1 + j\frac{ka}{4\pi Z_c}(3\zeta_0 \cos^2(\theta_0) + 4\pi Z_c)} \tag{A.16}$$

$$\approx \frac{\frac{4\pi Z_c}{jka}\frac{1}{3\zeta_0 \cos^2(\theta_0) + 4\pi Z_c} - 1}{\frac{4\pi Z_c}{jka}\frac{1}{3\zeta_0 \cos^2(\theta_0) + 4\pi Z_c} + 1}$$

$$= \frac{\frac{Z_A}{Z_c} - 1}{\frac{Z_A}{Z_c} + 1}$$

and so the antenna impedance Z_A corresponds to a capacitance C_A

$$Z_A(ka) = \frac{1}{j\,2\pi f C_A}$$

where

$$C_A = \frac{a(4\pi Z_c + 3\,\zeta_0 \cos^2(\theta_0))}{4\pi c Z_c^2} \tag{A.17}$$

From Equation A.12 and A.13, the effective length $h_e(f)$ is given by

$$kh_e(f) = -\frac{\exp(-jka) + \rho\exp(jka)}{ka\,(1-\rho)} \sum_{n\ odd}^{\infty} \frac{2n+1}{n(n+1)} \frac{j^{n-1}}{h_{n-1}^{(2)}(ka) - \frac{n}{ka} h_n^{(2)}(ka)} P_n$$

$$(\cos\theta_0)\frac{d}{d\theta}P_n(\cos\theta) \tag{A.18}$$

where the summation is over $n = 1, 3, 5, \ldots, N$. For electrically short monopoles ($ka << 1$), then only the $n = 1$ term need be considered in the summation, as for the antenna impedance. Using the approximation

$$h_0^{(2)}(ka) - \frac{1}{ka} h_1^{(2)}(ka) = 1 - \frac{j}{(ka)^3}$$

$$\approx -\frac{j}{(ka)^3}$$

the effective height for short conical monopoles can be calculated from

$$kh_e(f) = j\frac{3}{2}\frac{\exp(-jka) + \rho\exp(jka)}{ka\,(1-\rho)}(ka)^3 \cos\theta_0 \sin\theta$$

Using the approximation

$$\frac{\exp(-jka) + \rho\exp(jka)}{1-\rho} \approx \frac{1 - jka + \rho\,(1 + jka)}{1-\rho}$$

$$\approx \frac{1+\rho}{1-\rho} - jka$$

together with the approximation for ρ in (16) leads to

$$\frac{\exp(-jka) + \rho\exp(jka)}{1-\rho} \approx \frac{1}{j\frac{ka}{4\pi Z_c}(3\zeta_0\cos^2\theta_0 + 4\pi Z_c)} - j\,ka$$

$$\approx \frac{4\pi Z_c}{jka\,(3\zeta_0\cos^2\theta_0 + 4\pi Z_c)}$$

which yields the effective height

$$kh_e(f) = \frac{6\pi ka Z_c \cos\theta_0 \sin\theta}{4\pi Z_c + 3\zeta_0\cos^2\theta_0} \qquad \text{(A.19)}$$

A.5 Transfer Functions

Following the standard definition in [27] the transmission transfer function is defined as

$$T(f) = \frac{E_\theta(f)}{V_0(f)}$$

where E_θ is the electric field in the far field of the monopole and V_0 is the driving voltage. V_0 is related to I_0 in (12) by

$$I_0 = \frac{V_0}{Z_A + Z_L}$$

where Z_A is the antenna impedance and Z_L is the impedance of the feed line. Using Equation A.18, $T(f)$ is given by

$$T(f) = j\frac{\zeta_0 f}{cr}\frac{h_e(f)}{Z_A(f) + Z_L}\exp(-j2\pi fr/c) \qquad \text{(A.20)}$$

$$= T_0(f)\exp(-j2\pi fr/c)$$

$T_0(f)$ is clearly related to $T(f)$ with the phase delay due to the distance between the antenna and the far field point removed.

The reception transfer function $S(f)$ is defined in a similar fashion as

$$S(f) = \frac{V_L(f)}{E_{inc}(f)}$$

$$= \frac{h_e(f)\, Z_L(f)}{Z_A(f) + Z_L} \qquad \text{(A.21)}$$

where V_L is the load voltage across the antenna and E_{inc} is the incident field. The effective height can be calculated from Equation A.18 and the antenna impedance from Equation A.15 as a function of frequency.

For small monopoles with $ka << 1$ which are matched so that $Z_c = Z_L$, the approximate expressions for effective height Equation A.19 and antenna impedance Equation A.17 can be used in Equation A.20 and Equation A.21 to yield

$$T_0(f) = (j2\pi f)^2\frac{3\zeta_0 a^2\cos\theta_0\sin\theta}{4\pi Z_c rc^2} \qquad \text{(A.22)}$$

and

$$S(f) = j2\pi f\frac{3a^2\cos\theta_0\sin\theta}{2c} \qquad \text{(A.23)}$$

if the assumption $Z_A >> Z_L$ is made. This will be the most limiting assumption for the case of a 50 Ω monopole connected to a 50 Ω line.

The real and imaginary components of the transmission transfer function T_0 for a 50 Ω monopole with $\theta_0 = 46.98^o$ are plotted against ka in Figure A.2. The $1/r$ term in Equation A.20 has been suppressed. This plot is in agreement with Figure 13 from [27]. Figure A.3 shows the real and imaginary components of the reception transfer

function S(*f*) for 50 Ω conical monopoles. The agreement with Figure 16 of [27] is very good.

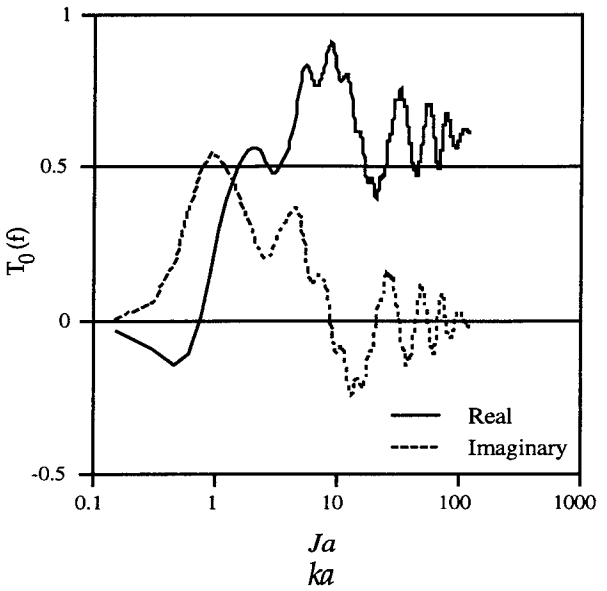

Figure A.2: Transmission transfer function of matched conical monopole

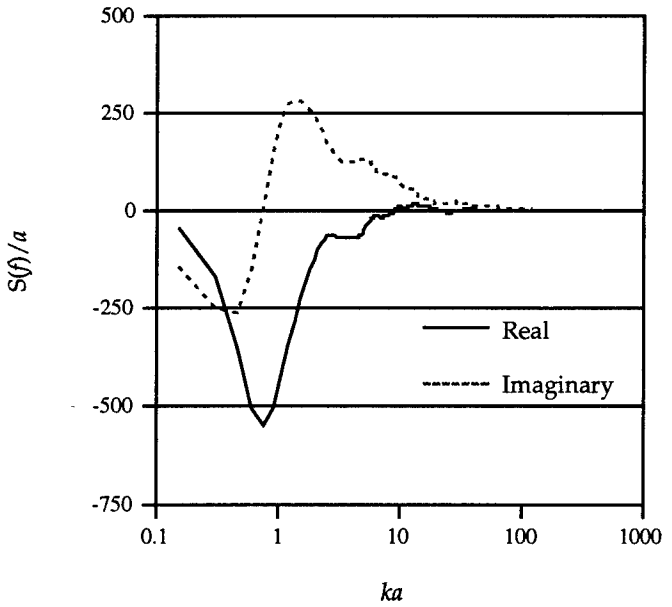

Figure A.3: Reception transfer function per unit antenna length for matched conical monopole

A.6 Time Domain Response

For transmit antennas, the time domain far field can be calculated from the applied voltage and the transmission transfer function using

$$e_\theta(t + r/c) = \int_{-\infty}^{+\infty} V_0(f)\, T_0(f)\, \exp(j2\pi ft)\, df$$

The frequency domain applied voltage is calculated from a time domain applied voltage using the Fourier transform

$$V_0(f) = \int_{-\infty}^{+\infty} v_0(t)\, \exp(-j2\pi ft)\, dt$$

For a Gaussian excitation pulse with a maximum of 1 V, the applied voltage $v_0(t)$ is given by

$$v_0(t) = \exp(-t^2/2\tau^2)$$

where $\tau = 0.4246\, t_w$, with t_w the FWHM for the pulse. The applied voltage in the frequency domain is

$$V_0(f) = \sqrt{2\pi}\, \tau\, \exp(-2\pi^2\tau^2 f^2)$$

For small monopoles, Equation A.22 can be used to relate the excitation voltage to the transmitted field in the time domain as

$$e_\theta(t + r/c) = \frac{3\zeta_0 a^2 \cos\theta_0}{4\pi Z_c r c^2} \frac{d^2 v_0(t)}{dt^2}$$

The radiated electric field for a number of antennas with different a/t_w values is shown in Figure A.4 for a Gaussian excitation pulse. As for Figure A.2, the $1/r$ term in the transmission transfer function has been suppressed. For large antennas as in Figure A.4 with $a/t_w = 6.62$, the radiated pulse is a faithful reproduction of the excitation pulse. For short antennas as for $a/t_w = 0.0883$, the radiated pulse is close to a double derivative of the excitation pulse. This is the result expected from the small monopole analysis. The results presented in Figure A.4 closely match those of Figure 5 in [27].

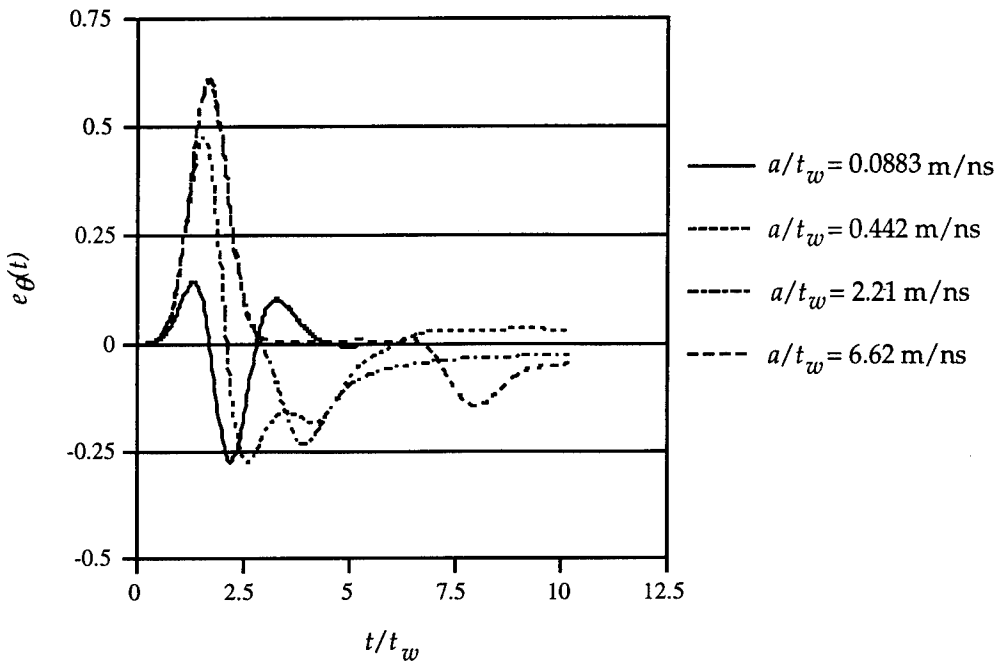

Figure A.4: Radiated field from 50 Ω conical monopole for various a/t_w.

The time domain load voltage in reception can be calculated from the incident field using the reception transfer function as follows

$$v_L(t) = \int_{-\infty}^{+\infty} E_{inc}(f)\, S(f)\, \exp(j2\pi ft)\, df$$

The incident electric field is calculated in a completely analogous way to the excitation voltage for transmission.

For small monopoles, Equation A.23 can be used to relate the incident field to the load voltage developed across the antenna in the time domain as

$$vL(t) = \frac{3a^2 \cos\theta_0}{2c} \frac{de_{inc}(t)}{dt}$$

The load voltage across conical monopoles for a negative Gaussian incident field with a peak of -1 V/m are shown in Figure A.5. Figure A.5 shows the response of a large monopole with a/t_w = 6.62 to be approximately the integral of the incident field. For a small monopole, the response is proportional to the derivative of the incident field, as for a/t_w = 0.0883. This is expected from the small monopole analysis. The results shown in Figure A.5 are in close agreement with those presented in Figure 10 of [27].

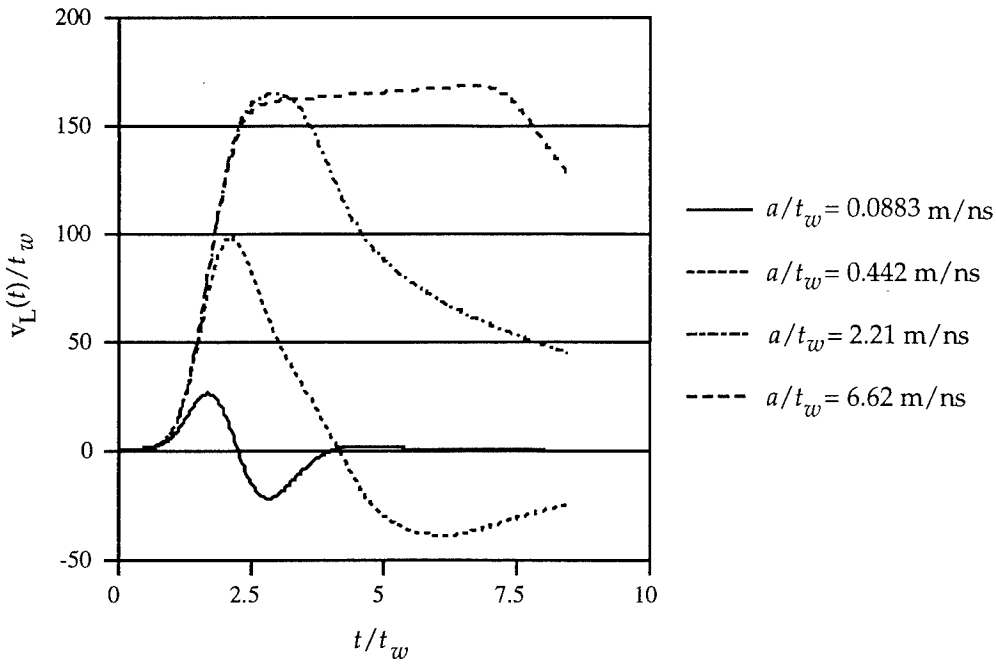

Figure A.5: Voltage across 50 Ω conical monopole receive antenna for various a/t_w.

A.7 Summary

The results presented in this appendix show conclusively that the analytic theory of [25-27] has been successfully reproduced, and that the approximations are identified. The most serious approximation is the inclusion of only the TEM mode within the antenna, with higher order evanescent modes neglected completely inside the antenna. Of secondary importance, it is assumed that there are no reflections from the feed. This approximation is significant when calculating the high frequency response of the antenna, since the feed geometry is the limiting factor. This is particularly important for the analysis of high power antennas where the feed is generally made as large as possible without degrading the high frequency response of the antenna beyond an acceptable limit.

The simple expressions for the antenna impedance and effective height of small monopoles with $ka << 1$ presented in [27] were derived. These simple approximations have been used to calibrate small antennas such as D-dot sensors. If the further approximation that the antenna impedance is much larger than the load impedance, then simple time domain expressions relating the incident field and load voltage for reception and the excitation voltage and radiated field for transmission could be derived. This last approximation is the most limiting in terms of the minimum pulse widths that can be accurately modelled using these approximate time domain formulae.

A.8 References

[1] G. Staines, "High-power microwave (HPM) technology - Part I Pulsed power for HPM systems," *ERL-0711-RN*, June 1993.

[2] G. Staines, "High-power microwave (HPM) technology - Part II Relativistic electron beam devices," *ERL-0712-RN*, June 1993.

[3] G. Staines, "High-power microwave (HPM) technology - Part III Generating high-power microwaves without electron beams," *ERL-0713-RN*, June 1993.

[4] G. Staines, "High-power microwave (HPM) technology - Part IV Military applications of high-power microwaves," *ERL-0714-RN*, June 1993.

[5] H. Helava, M. Herman, C. Leung, J. Oicles, L. Ragle, S. Wessman, A. Falk, J. Adams, S.J. Davis, "Bulk avalanche semiconductor switches (BASS) for high resolution ultra-wideband radar (UWBR) applications," *SPIE Ultrahigh Resolution Radar*, Vol. 1875, 1993, pp. 14-22.

[6] "0.5 megawatt, ultra-wideband pulse generator," *Microwave Journal*, Sep 1993, pp. 165-166.

[7] G.A. Mesyats, V.G. Shpak, M.I. Yalandin, S.A. Shunailov, "Compact high-current repetitive pulse accelerators," *Proceedings of the 8th Pulsed Power Conference*, 1991, pp. 73-77.

[8] M.I. Yalandin, G.A. Mesyats, V.G. Shpak, G.T. Smirnov, S.A. Shunailov, "Repetitive 4-millimeter-range back-wave oscillator," *SPIE Intense Microwave Pulses*, Vol. 1872, 1993, pp. 333-342.

[9] S.M. Rao, D.R. Wilton, "Transient scattering by conducting surfaces of arbitrary shape," *IEEE Transactions on Antennas and Propagation*, Vol. 39, No. 1, Jan 1991, pp. 56-61.

[10] D.A. Vechinski, S.M. Rao, "A stable procedure to calculate the transient scattering by conducting surfaces of arbitrary shape," *IEEE Transactions on Antennas and Propagation*, Vol. 40, No. 6, June 1992.

[11] K.S. Yee, "Numerical solution of initial boundary value problems involving Maxwell's equations in isotropic media," *IEEE Transactions on Antennas and Propagation*, Vol. AP-14, May 1966, pp. 302-307.

[12] J.G. Maloney, G.S. Smith, W.R. Scott, "Accurate computation of the radiation from simple antennas using the finite-difference time-domain method," *IEEE Transactions on Antennas and Propagation*, Vol. 38, No. 7, July 1990.

[13] P.J. Hum, M.S. Leong, P.S. Kooi, T.S. Yeo, S.P. Yeo, "Finite-difference time-domain (FD-TD), analysis of centre-driven circular microstrip antennas with finite ground plane," *1992 Asia-Pacific Microwave Conference Proceedings*, pp. 297-299.

[14] D.E. Merewether, "Transient currents induced on a metallic body of revolution by an electromagnetic pulse," *IEEE Transactions on Electromagnetic Compatibility*, Vol. EMC-13, No. 2, May 1971, pp. 41-44.

[15] D. Lamensdorf, L. Susman, "Baseband-Pulse-Antenna Techniques," *IEEE Antennas and Propagation Magazine*, Vol. 36 No. 1, Feb 1994, pp. 20-30.

[16] A.C. Cangellaris, D.B. Wright, "Analysis of the numerical error caused by the stair-stepped approximation of a conducting boundary in FDTD simulations of electromagnetic phenomena," *IEEE Transactions on Antennas and Propagation*, Vol. 39, No. 10, Oct 1991, pp. 1518-1525.

[17] T.G. Jurgens, A. Taflove, K. Umashankar, T.G. Moore, "Finite-difference time-domain modelling of curved surfaces," *IEEE Transactions on Antennas and Propagation*, Vol. 40, No. 4, April 1992, pp. 357-366.

[18] R.J. Luebbers, K.S. Kunz, M. Schneider, F. Hunsberger, "A finite-difference time-domain near zone to far zone transformation," *IEEE Transactions on Antennas and Propagation*, Vol. 39 No. 4, April 1994, pp 848-851.

[19] S. Ramo, J.R. Whinnery, T. van Duzer, *Fields and Waves in Communication Electronics*, 2nd *edition*, 1984, pp 607-609.

[20] K.S. Yee, D. Ingham, K. Shlager, "Time-domain extrapolation to the far field based on fdtd calculations," *IEEE Transactions on Antennas and Propagation*, Vol. 39 No. 3, March 1991, pp 410-413.

[21] J.G. Maloney, G.S. Smith, "Optimization of a conical antenna for pulse radiation: an efficient design using resistive loading," *IEEE Transaction on Antennas and Propagation*, Vol. 41 No. 7, July 1993, pp 940-947.

[22] D.M. Parkes, P.D. Smith, "Practical method of predicting transient fields and monopole current waveforms," *IEE Proceedings*, Vol. 135 Pt. H No. 4, August 1988, pp 231-236.

[23] J.A. Stratton, *Electromagnetic Theory*, McGraw-Hill, 1941, p. 417.

[24] M. Abramowitz, I.A. Stegun, Ed., *Handbook of Mathematical Functions*, Dover, 1970, pp. 332-333.

[25] C.H. Papas, R.W.P. King, "Input impedance of wide-angle conical antennas fed by a coaxial line," *Proceedings of the IRE*, Vol. 37, Nov 1949, pp. 1269-1271.

[26] C.H. Papas, R. King, "Radiation from wide-angle conical antennas fed by a coaxial line," *Proceedings of the IRE*, Vol. 39, Jan 1951, pp. 49-51.

[27] C.W. Harrison, C.S. Williams, "Transients in wide-angle conical antennas," *IEEE Transactions on Antennas and Propagation*, Vol. AP-13 No. 3, May 1965, pp. 236-246.

THIS PAGE INTENTIONALLY BLANK

A Finite Difference Time Domain Calculation for Rotationally Symmetric Ultrawideband Antennas

Geoff Staines and Sean Braidwood

(DSTO-RR-0019)

DISTRIBUTION

	Number of Copies
DEPARTMENT OF DEFENCE	
Defence Science and Technology Organisation	
Chief Defence Scientist and members of the	) 1 shared copy
DSTO Central Office Executive	) for circulation
Counsellor Defence Science, London	Doc Control Data Sheet Only
Counsellor Defence Science, Washington	Doc Control Data Sheet Only
Scientific Adviser POLCOM	1
Senior Defence Scientific Adviser	1
Assistant Secretary Scientific Analysis	1
Director, Aeronautical and Maritime Research Laboratory	1
Chief, Weapons Systems Division	1
Defence Intelligence Organisation	
Director, Scientific Analysis Branch. Att. Head, Electronics	1
Electronics and Surveillance Research Laboratory	
Director, Electronic and Surveillance Research Laboratory	1
Chief, Communications Division	1
Chief, High Frequency Radar Division	1
Chief, Information Technology Division	1
Chief, Microwave Radar Division	1
Chief, Electronic Warfare Division	1
Research Leader, Electronic Countermeasures	1
Head, Advanced Concepts Group	1
Dr Bevan D. Bates, Advanced Concepts Group	1
Dr Geoff W. Staines, Advanced Concepts Group	1
Mr Sean W. Braidwood, Advanced Concepts Group	1
HQADF	
Director, Directorate of Communications Engineering	1
Director General, Force Development (Sea)	1
Director General, Force Development (Air)	1

Director General, Force Development (Land)	1
Director General, Force Development (Joint)	1
Navy Office	
Navy Scientific Adviser	1
Army Office	
Scientific Adviser - Army	1
Air Office	
Air Force Scientific Adviser	1
DIO	
Dirwctor ,Scientific Analysis Branch. Att. Head, Electronics	1
Libraries and Information Services	
Defence Central Library, Technical Reports Centre	1
Manager, Document Exchange Centre (for retention)	1
National Technical Information Services, United States	2
Defence Research Information Centre, United Kingdom	2
DRA Malvern, UK. Att Mr D. M. Parkes	1
Defence Science and Technology Organisation Salisbury, Research Library	2
Library Defence Signals Directorate, Canberra	1
Spares, DSTOS, Research Library	6

Department of Defence

DOCUMENT CONTROL DATA SHEET

1. Page Classification	UNCLASSIFIED
2. Privacy Marking/Caveat	

3a. AR Number	3b. Establishment Number	3c. Type of Report	4. Task Number
AR-008-994	DSTO-RR-0019	RESEARCH REPORT	ADF 93/284

5. Document Date	6. Cost Code	7. Security Classification	8. No. of Pages	76
FEBRUARY 1995	839262	[L] [U] [U]	9. No. of Refs.	27

Document Title Abstract

S (Secret C (Confi) R (Rest) U (Unclass)

* For UNCLASSIFIED docs with a secondary distribution LIMITATION, use (L) in document box.

10. Title

A FINITE DIFFERENCE TIME DOMAIN CALCULATION FOR ROTATIONALLY SYMMETRIC ULTRAWIDEBAND ANTENNAS

11. Author(s)

Geoff Staines
Sean Braidwood

12. Downgrading/ Delimiting Instructions

Limitation to be reviewed in February 2000

13a. Corporate Author and Address

Electronic Warfare Division
Electronics and Surveillance Research Laboratory
PO Box 1500 SALISBURY SA 5108

13b. Task Sponsor

HQADF

14. Officer/Position responsible for

Security	SOESRL
Downgrading	CEWD
Approval for release	CEWD

15. Secondary Release Statement of this Document

~~Access additional to the initial distribution is limited to the Defence Community of Australia, US and UK. Others MUST be referred to Chief, Electronic Warfare Division, ESRL.~~

Any enquiries outside stated limitations should be referred through DSTIC, Defence Information Services, Department of Defence, Anzac Park West, Canberra, ACT 2600.

16a. Deliberate Announcement

May be announced to the Defence Community of Australia, UK and USA

16b. Casual Announcement (for citation in other documents)

[√] No Limitation | [ ] Ref. by Author, Doc No and date only

17. DEFTEST Descriptors

Biconical Antennas
Electronic Countermeasures
Microwave Antennas
Radar Antennas
Broadband Antennas

18. DISCAT Subject Codes

0049A

19. Abstract

A finite difference time domain (FDTD) technique for the analysis of ultrawideband (UWB) antennas with rotational symmetry has been developed. The theory is intended to treat various types of biconical antennas, and a mode matching analysis of spherically-capped bicones has been performed to verify the correct implementation of the FDTD calculation. In addition, experimental results have been obtained which are compared to the theoretical results. The FDTD software can be used for the design of high-power, directive UWB antennas with low sidelobe leakage for high-power UWB radar and electronic countermeasures applications.

ADB 205827

DEPARTMENT OF DEFENCE
DEFENCE SCIENCE & TECHNOLOGY ORGANISATION
DSTO

SCIENCE CORPORATE MANAGEMENT BRANCH
DSTO RESEARCH LIBRARY-REPORTS DISTRIBUTION
PO BOX 1500 EDINBURGH SA 5111

Reference: R9607/7/9 Pt4 Folio No.82
Contact: Natalie Mahlknecht
E-mail: Natalie.Mahlknecht@dsto.defence.gov.au

Telephone: (08) 8259 6255
Facsimile: (08) 8259 6803

Tuesday, 26 March 2002

To All Copyholders
cc: To the Team Leader of Records & Archives

Notification of Downgrading/ Delimiting of DSTO Report

Please note that the Release Authority has authorised the downgrading/ delimiting of the report detailed here:

DSTO NUMBER	**DSTO-RR-0019**
AR NUMBER	**AR-008-994**
FILE NUMBER	**Unknown**
PREVIOUS Classification	**WAS:-** LIMITED RELEASE
REVISED Classification and Release Limitation	UNCLASSIFIED **Public Release** **NO LIMITATIONS**

Please amend your records and make changes to your copy of the report itself to reflect the new classification/ release limitation.

Mrs. Natalie Mahlknecht
Reports Distribution Officer
DSTO Research Library, Edinburgh